Fault sealing and caprock integrity for CO_2 storage: an in-situ injection experiment

Alba Zappone[1,2], Antonio Pio Rinaldi[1,6], Melchior Grab[3], Quinn C. Wenning[3], Clément Roques[3,4], Claudio Madonna[2], Anne C. Obermann[1], Stefano M. Bernasconi[3], Matthias S. Brennwald[5], Rolf Kipfer[5], Florian Soom[6], Paul Cook[6], Yves Guglielmi[6], Christophe Nussbaum[7], Domenico Giardini[3] , Marco Mazzotti[2], Stefan Wiemer[1]

[1]Swiss Seismological Service, ETHZ, Zurich, 8092, Switzerland
[2]Department of Mechanical and Process Engineering, ETHZ, Zurich, 8092, Switzerland
[3]Department of Earth Sciences, ETHZ, Zurich, 8092, Switzerland
[4]Univ Rennes, CNRS, Géosciences Rennes, UMR 6118, 35000 Rennes, France
[5] Department of Water Resources and Drinking Water, EAWAG Dübendorf, 8600, Switzerland
[6]Energy Geosciences Division, LBNL Berkeley, CA 94720, USA
[7]Swiss Geological Survey, swisstopo, Wabern, 3084, Switzerland

Correspondence to: Alba Zappone (alba.zappone@sed.ethz.ch)

Abstract. The success of geological carbon storage depends on the assurance of a permanent containment of the injected carbon dioxide (CO_2) in the storage formation at depth. One of the critical elements of the safekeeping of CO_2 is the sealing capacity of the caprock overlying the storage formation, despite faults and/or fractures, which may occur in it. In this work, we present an ongoing injection experiment performed in a fault hosted in clay at the Mont Terri underground rock laboratory (NW Switzerland). The experiment aims at improving our understanding on the main physical and chemical mechanisms controlling i) the migration of CO_2 through a fault damage zone, ii) the interaction of the CO_2 with the neighbouring intact rock, and iii) the impact of the injection on the transmissivity in the fault. To this end, we inject a CO_2-saturated saline water in the top of a 3 m thick fault in the Opalinus Clay, a clay formation that is a good analogue of common caprock for CO_2 storage at depth. The mobility of the CO_2 within the fault is studied at decameter scale, by using a comprehensive monitoring system. Our experiment aims to the closing of the knowledge gap between laboratory and reservoir scales. Therefore, an important aspect of the experiment is the decameter scale and the prolonged duration of observations over many months. We collect observations and data from a wide range of monitoring systems, such as a seismic network, pressure temperature and electrical conductivity sensors, fiber optics, extensometers, and an in situ mass spectrometer for dissolved gas monitoring. The observations are complemented by laboratory data on collected fluids and rock samples. Here we show the details of the experimental concept and installed instrumentation, as well as the first results of the preliminary characterization. Analysis of borehole logging allow identifying potential hydraulic transmissive structures within the fault zone. A preliminary analysis of the injection tests helped estimating the transmissivity of such structures within the fault zone, as well as the pressure required to mechanically open such features. The preliminary tests did not record any induced microseismic events. Active seismic tomography enabled a sharp imaging the fault zone.

KEYWORDS: CO_2 STORAGE: CO_2 INJECTION, CAPROCK INTEGRITY, SITE MONITORING, IN-SITU DECAMETER SCALE EXPERIMENT

1 Introduction

Carbon Capture and Storage (CCS) has a fundamental role to reduce the content of anthropogenic CO_2 in the atmosphere and to achieve the Paris Agreement's challenging objective of keeping a global temperature rise below 2°C above pre-industrial levels (IPCC 2018, 2019; Cozier, 2015).

Carbon storage at mega-tons scale has been proven successful (e.g., Sleipner, Snøhvit, Weyburn, Aquistore, Quest), but needs to be increased to giga-tons scale in order to achieve global emissions reductions targets (IPCC, 2018; Zoback & Gorelick,

2012). Achievement of this upscaling is critically linked to better estimates of storage capacity and improved risk management strategies that rely on detailed monitoring with combined geophysical, geochemical, and hydrogeological methods (e.g. Aagaard et al., 2018; Fang et al., 2010; Rutqvist, 2012). One of the challenges both in evaluating the storage capacity and in pressure-managing strategies is the assessment of long-term integrity of sealing formations. CO_2 leakage along potential high permeability pathways into near-surface aquifers or to the surface is potentially one of the main geological hazard for CCS that might challenge the technical feasibility and the social and political acceptability of the whole technology (Zoback and Gorelick, 2012).

Faults within the caprock represent one of the possible pathways for CO_2 to migrate out of the storage reservoir. The presence of faults will greatly affect the site characterization process in terms of safety assessment, and consequently of monitoring plan, and risk management (prevention, mitigation, remediation actions). Faults are also key elements in the evaluation of induced seismicity risk during injection operations (Rutqvist et al., 2016). It was argued that the injection of large volumes of CO_2 at relatively shallow depth (few km) in brittle rocks could trigger earthquakes (Zoback and Gorelick, 2012), although injecting in soft sedimentary basin (Vilarrasa and Carrera, 2015) might reduce such potential risk. However, if earthquakes, even of modest magnitude, can damage the caprock and jeopardize its sealing capacity, CCS may result in an unsuccessful strategy for significantly reducing greenhouse gas emissions (Zoback and Gorelick, 2012).

Fault internal structure, mechanical properties and fluid flow are inextricably coupled (Caine et al., 1996; Faulkner et al., 2010; Bush & Kapmann, 2018). Despite fault zone complexity, a close coupling exists between thermal, hydraulic, mechanical, and chemical processes in fractures and faults. Several studies have focused on understanding the geomechanical processes related to CO_2 injection, at both lab and field scale (Vilarrasa et al., 2019 and references herein). Often caprock failure has been linked to changing thermo-hydro-mechanical (THM) processes. Numerical simulations have highlighted how fault/fracture reactivation in caprocks are affected by two-phase fluid flow (Jha and Juanes, 2014), the presence of heterogeneities (Rinaldi et al., 2014), or temperature changes (Vilarrasa et al., 2017). Field studies on deformation (Vasco et al., 2010; Vasco et al., 2018) corroborated by numerical modelling (Gemmer et al., 2012; Shi et al., 2013; Rinaldi & Rutqvist, 2013; Rinaldi et al., 2017), have highlighted the importance of potential caprock failure on successful CO_2 storage. The coupling between chemical and mechanical processes have been studied in the laboratory (Le Guen et al., 2007; Hangx et al., 2013; Amann et al, 2017; Vialle & Vanorio, 2011; Mikhaltsevitch et al., 2014) and through field evidence (Rinehart et al., 2016; Hovorka et al, 2013; Al Hosni et al., 2016; Skurtveit et al., 2018), mostly for storage reservoir rocks. These geochemical reactions could influence other characteristics of the rocks (e.g., mechanical parameters), which can in turn be linked to fault reactivation and induced seismicity (Vilarrasa & Makhnenko, 2017). A limited set of experimental studies have reported on the chemical processes that occur in caprocks, such as clays, shales and carbonate rich shales (Kaszuba et al., 2005; Credoz et al., 2009; Alemu et al., 2011; Kapman et al., 2016), highlighting a relevant knowledge gap when it comes to successful CO_2 storage.

A large amount of empirical observations is provided by CO_2 injection operations conducted by oil and gas industry (e.g. Jia et al., 2019, Michael et al., 2010 and references therein), but experiments targeting faults, especially on geomechanical and geochemical coupling are still quite rare. Over the past decade a few in situ-scale experiments have been conducted on controlled release of CO_2 (free phase or dissolved) to better understand environmental impacts and test monitoring techniques (Roberts & Stalker, 2017, and references therein). The experiments differ in many aspects, such as geological environments, injection depth and injection strategy. Most experiments released CO_2 into unconsolidated formations such as sand or gravel, with only one exception to date, where gaseous CO_2 was injected into a lithified carbonate formation at only 3 m depth (Rillard et al., 2015). These experiments usually mimic the effects of leakage from wells by injecting into a vertical structure from a point source. The leakage through a fault is simulated by injecting from a linear feature. Besides the experiment described in this contribution, to the best of our knowledge only two other test-sites, the CISIRO In-Situ Laboratory Project in Western Australia (Myers et al., 2020 and references herein) and the CO2CRC at Otway National Research Facility in Victoria, Australia (Feitz et al., 2018; Tenthorey et al., 2019), foresee experiments of controlled release of CO_2 at shallow depth. The Project in Western Australia targets a fault in a reservoir formation with the injection of a small volume of CO_2, with the purpose to evaluate the ability to monitor and detect unwanted leakage of carbon dioxide from a storage complex (Michael et al., 2019). The Western Australian experiment is ongoing as injection started in early 2019 (K. Michael, pers. comm.). The experiment at Otway Research Facility has reached the stage of completed site characterization and design of the monitoring system, while the experiment performing shallow release of CO_2 will take place in the coming months (Feitz et al., 2018; Tenthorey et al., 2019).

Recently the Mont Terri rock laboratory (MTRL) hosted a decameter scale experiment (FS experiment), aiming at observing the rupture and sliding mechanisms on a fault subjected to injections of large amounts of fluid. The FS experiment aims at understanding the conditions for slip activation and stability of clay faults, and the evolution of the coupling between fault slip, pore pressure and fluids migration. The experiment revealed complex rupture mechanism associated to micro seismicity (e.g. Guglielmi et al. 2020a, b). Results obtained in the course of the experiment are crucial in defining mechanisms of natural and induced earthquakes, their precursors and risk assessment. The FS test and its findings constitute a valid basis to develop the experiment we describe in this work.

However, experiments that aim at investigating the transport and migration of CO_2 in caprock formations at decameter scale under controlled conditions (i.e., confining pressure, pore pressure, temperature, saturation degree, etc.) are still rare. To the best of our knowledge, the only experiment to date dealing with an injection prolonged for many months was conducted at Daniel Electric Generating Plant, Mississippi, and specifically targeted the effects of dissolved CO_2 on shallow groundwater reservoir, and not on the transport and migration of CO_2. Hence, the testing of faulted caprocks subjected to CO_2 injection and the monitoring of coupled geomechanical and geochemical effects is of particular interest, because it offers direct observations

that will help to gain insight into coupled THMC processes in faulted caprock and ultimately to improve site assessments of storage sites.

We are currently running an experiment that aims at covering this knowledge gap by providing observations on CO_2 migration in a fault system, at a decameter scale, therefore under well-controlled conditions, but targeting a rock volume that can capture heterogeneities representative of a large scale in-situ injection. We want to simulate a situation in which the CO_2 contained in a storage site reaches a caprock that is crosscut by faults. We want to target one of the most critical conditions, when CO_2 could escape the reservoir through the fault, and possibly contaminate fresh water aquifers in the overburden or/and reach the surface and release to the atmosphere (Fig. 1). The MTRL located in northwester Switzerland (Fig. 2), allows in-situ access to a fault (Mont Terri Main Fault) hosted in a clay formation, the Opalinus Clay, and offers a unique opportunity for a prolonged (multiple months) decameter-scale CO_2 injection experiment (CS-D: Carbon Sequestration - Series D) into a fault to study relevant geomechanical and geochemical processes on leakage and fault properties.

This paper presents the concept of the CS-D, a general overview of the CS-D test-site, the conceptual design and the details of the experimental instrumentation. We also present results from the characterization of the rock volume prior to CO_2 injection, which provided the parameters adopted for the continuous long-term CO_2 injection that is currently ongoing. Finally, we discuss the implication of the current observations, and speculate on the potential impact of the long-term experiment.

2 Overview of the Experiment

The general concept of the CS-D experiment is to introduce CO_2-saturated water and tracers in the fault at MTRL, in a long-term (12 months) steady state continuous injection, forerun and intercalated by short, pulse-wise, pressure increase steps that would be repeated at regular intervals during the long-term injection. The effects of the injection are monitored by a synchronized complex monitoring system that is described in detail in section 3.3.

2.1 Aims

With the CS-D experiment, we want to understand how exposure to CO_2 affects the sealing integrity of a caprock hosting a fault, through observation on permeability changes, on fluid migration along the fault, and on interaction with the surrounding environment. With this we want to test the hypothesis that the retention capacity of the rock, even if faulted, is not affected by exposure to CO_2 if the pressure conditions are not causing fault rupture. We also want to test the hypothesis of self-sealing of the fault after eventual rupture and slip events. We want to investigate the concerns expressed by Zoback and Gorelick (2012) that the sealing integrity of CO_2 repositories can be threatened by earthquakes even of small size, and to which extent the concern can be generalized. Finally, we want to validate instrumentation and methods for monitoring and imaging fluid

transport, we want to generate well-constrained parameters as inputs for Hydro-Mechanical-Chemical (HMC) simulations, and validate the observation on the mobility of CO_2 in the caprock and the possibility of leakage in the overburden.

With the CS-D experiment, we aim at better understanding the processes governing:

1. the mobility of CO_2-rich water through the damaged zones of a fault;
2. the impact of long-term (ca. twelve months) exposure to CO_2-rich water on the permeability/porosity in the damaged zone and in the intact rock;
3. the coupled geochemical and geomechanical variations due to rock-water interaction;
4. the propagation of the transient field pressure in the fault and in the host-rock;
5. the deformation of the rock mass as response to pressurization and slip, if any;
6. the occurrence of induced micro-seismicity in clay.

With its dense network of monitoring systems, the experiment aims at collecting multiparameter observations and data from independent but strongly integrated monitoring techniques. Over the course of the experiment, we aim to establish a dataset at high spatial resolution that will yield insight into the interrelationship of hydraulic, geomechanical, and geochemical processes within the fault. Therefore, a dense network of multi-parameter sensors is installed around the injection site, to monitor the rock volume hosting the fault zone. The installation of the CS-D experiment in MTRL includes micro-seismicity and active seismic monitoring, cross-hole electrical resistivity monitoring, axial deformation, coupled with a three-dimensional displacement probe (SIMFIP, Guglielmi et al., 2013), and in-situ dissolved gases monitoring. The installation of a permanent infrastructure allows for long-term experiments.

Direct laboratory measurements on rock and fluid samples at centimeter scale are also an essential part of the experiment. The aim is to integrate the geophysical observation with analytical tests both on fluid samples collected within the fault and on rock samples either from the fault or from the intact rock. Samples from intact rock and fault zone collected before and after the injections will allow characterization of mineralogical and chemical changes due to the rock-fluid interaction; geomechanical tests will reveal possible changes due to exposure to CO_2-rich water. This part is not discussed in the present paper and a detailed description of the methodology adopted for lab studies is reported in Wenning et al., 2019.

Numerical modelling assists the design and analysis of different phases of the experiment, and a primary aim of the experiment is also to provide parameters to calibrate numerical models that can be used for enhancing process understanding, sensitivity studies and upscaling.

The CS-D experiment takes advantage from close cooperation with a partner experiment, FS-B (Guglielmi et al., 2019), at a nearby location, also injecting fluids into faults, but having complementary objectives:

- The FS-B's main aim is to imaging fluid flow, permeability and stress variations during rupture along the Main Fault zone, to better understand the role of fluids in earthquake rupture and fault reactivation. The experiment will feature large injection volumes, and long-term monitoring of the recovery phase.
- The CS-D experiment discussed in this work focuses on the role of CO_2-rich water on hydro-mechanical-chemical properties and addresses the long-term behaviour of clays exposed to several months of low flow rate injection.

The time schedule of the two projects is closely coordinated. Because the FS-B experiment will stimulate the same fault targeted by the CS-D injection, it simulates the case of a seismic event causing a rupture and a slip, and gives the opportunity to the CS-D motoring equipment to record the event and to detect possible leakages due to the slip. The FS-B stimulation is planned at a late stage of the CS-D experiment, after a long-term injection phase in CS-D, when the observation of the evolution of the CO_2 in the fault indicates a steady-state flow path.

2.2 Location

The MTRL is an underground facility located in northwestern Switzerland (Fig. 2a) in the Jura Mountains, a small fold-and-thrust belt (Fig. 2c) that represents the youngest and most external deformation zone of the Alps (Pfiffner, 2014). The laboratory is located 280 m below the surface and comprises c.a. 700 m of galleries and niches.. The MTRL, under the responsibility of the Swiss Geological Survey, swisstopo, hosts experiments of twenty-two organizations from various countries worldwide, and offers a technical and scientific platform facilitating the realization of scientific projects in the field of deep geological disposal.

Experiments in the MTRL investigate the properties of a pristine claystone, the Opalinus Clay, that has been indicated as a possible host rock for radioactive waste in Switzerland (Bossart et al., 2017 and references therein). Because of its very low hydraulic permeability and its regional extension over the Swiss Molasse basin, the formation is also considered a good seal for underground reservoirs (i.e., CO_2 storage) at the regional scale.

The Opalinus Clay, is sequence of shale deposited around 174 Ma ago (Hostettler et al. 2017). It has been sub-divided into three main facies, clayey, sandy and carbonate-rich (Blaesi et al. 1996; Hostettler et al. 2017), on the basis of the content of clay minerals, quartz and carbonate. It is an overconsolidated clay, which has reached an estimated maximum burial depth of around 1350 m at the current laboratory area, with an overconsolidation ratio of almost 5, assuming a current average overload of 280 m (Hostettler et al. 2017). The formation is 131 m thick (Bossart et al., 2017) at the MTRL. The Opalinus Clay and the adjacent formations form an anticline, crosscut by the tunnels of the lab. This structure is interpreted as a fault-bend fold, where a series of thrust faults, extensional faults, and strike-slip faults intersect in a complex pattern (Nussbaum et al. 2011).

Among these tectonic features, the most evident is the so called Main Fault, a thrust fault, located in the shaly-facies, with shear movement towards NNW (Nussbaum et al., 2011). The Fault zone consists of several architectonic elements: fault gouge, S–C bands, meso-and micro-scale folds, numerous intersecting fault planes, and apparently undeformed volumes. The thickness of the fault zone varies between 1 and 4.5 m (Nussbaum et al., 2011).

The CS-D experiment takes place across the Main Fault, accessed from the newly excavated niche 8 (Fig. 2 b). The niche is located entirely in the shaly-facies of the Opalinus Clay. A set of vertical and inclined boreholes have been drilled and instrumented from niche 8 going through the fault zone.

2.3 Timeline

The CS-D experiment comprises three main phases (Fig. 3).

- **Phase 1**: preparation of the long-term injection phase. It included the planning, and realization of the experimental infrastructure: drilling of boreholes, logging, collection and storage of samples, boreholes completion and instrumentation, installation of surface geophysical monitoring equipment and all ancillary operations aimed at completion of the experimental infrastructure. Moreover, in this phase we characterized the rock volume in terms of geological and structural features, hydraulic properties, and seismic velocity distribution, all of which are essential for the design of the long-term fluid injection and the interpretation of the experimental results. During the first phase, one main goal was to define the long-term injection pressure. To this end we performed repeated hydraulic tests in order to define the pressure at which the fault suddenly shows a large increase of flow rate for small pressure increments, otherwise known as the Fault Opening Pressure (FOP, Guglielmi et al.2016). The concept of FOP, defined as the pressure threshold at which a large increase in flow rate is registered at the injection point, and considered the start of activation of the fault (Guglielmi et al., 2016), was particularly helpful in designing the CS-D injection protocol. We performed these tests in different injection intervals within the fault in order to determine what, if any, zones are more reactive to pressure changes, and plan the installation of fluid sampling and monitoring equipment. The experimental installation was performed from August to December 2018. Baseline acquisition started immediately after the installation completion and lasted until May 2019. The results of these baseline measurements are presented in this paper.
- **Phase 2**: long steady state injection, below the FOP. We inject CO_2-saturated water and tracers while we keep monitoring pressure, electrical resistivity and pH, seismic velocity changes, and gas content. Water is sampled from the fault at regular time intervals and analysed in laboratories to monitor for chemical variations. In this phase, we regularly repeat hydraulic tests and compare the results to detect possible variation in the fluid mobility. The long-term constant pressure injection with CO_2-saturated water started in June 2019. This phase will be terminated when

the neighbour experiment FS-B takes place (at present still pending). The FS-B experiment will inject large quantities of water at high pressure at a distance of c.a. 20 m from CS-D injection point, aiming at substantially increasing the permeability of the fault zone.

- **Phase 3**: post long-term injection operations. We will repeat the characterization tests and prolonged injection test to identify possible effects of the FS-B experiment on the CS-D injection site. This phase may also include the collection of rocks cores from sampling drills that will reach the volume exposed to CO_2-saturated water, for further detailed petrophysical, geo-mechanical, and geochemical characterization at the lab scale. A new long-term injection phase is foreseen to highlight possible changes in leakage rate after a major fault zone stimulation.

All the phases are integrated by continuous monitoring pressure, deformation, pH and water electrical conductivity, as described in detail in the following section 3.3.

3 Layout of the installation

The layout of the boreholes used in the CS-D experiment was determined from constraints defined by the geometry of the fault, by bedding of the clay and by preliminary numerical modelling of fluid flow, aimed at defining the position of the boreholes and ensuring accuracy of the monitoring instrumentation. To avoid interference from the excavation damage zone (EDZ) around the tunnel, we planned the injection boreholes and the fluid monitoring borehole to intersect the fault at a depth greater than 10 m, given the tunnel radius of 5 m (Bossart et al., 2002).

The position and geometry of the Main Fault was the basis to start the planning of the experimental layout. The depth of the fault was preliminarily calculated through the 3D geological model, provided by swisstopo. The Main Fault is primarily strike oriented N80° and dipping ~50-65 °SE. From the fault geometry model, we expected the fault to be approximately 10 to 25 meters below niche 8, increasing in depth towards the southern end of the niche, well below the EDZ (Fig. 5a). During the drilling phase, core mapping and borehole image logs provided more precise understanding of the Main Fault geometry and allowed for adaptations to the borehole positioning.

3.1 Numerical scoping calculations

Preliminary numerical modelling results with the coupled numerical simulator TOUGH-FLAC (Rutqvist, 2011; Rinaldi & Rutqvist, 2019) helped constrain the distance between injection and monitoring boreholes. Such simulator allows solving for coupled fluid flow and geomechanics. For planning, we tested scenarios with both constant and stress-dependent permeability. Similar to previous numerical modelling of the FS experiment (Guglielmi et al., 2020a,b), the injection occurs with constant head at the centre of a 20×20×20 m domain and with a planar feature representing the fault zone (Fig. 4a). The fault plane, embedded in a 3D model, is simulated with a finite width (1 m). The preliminary model assumed an injection strategy similar

to the previous FS-experiment (Guglielmi et al., 2020), where the injection time was extended to account for a long-term injection (twelve months, given some preliminary planning of the experiment – Fig. 4b). The main goal of this preliminary modelling was to assess the maximum reach of the pressure front and of the injected water.

In a first set of simulations, we assumed that the permeability would remain constant during injection. We considered permeability values ranging from 10^{-21} to 10^{-19} m^2; therefore, we simulated cases with permeability slightly larger and slightly smaller than the value found in literature (Marschall et al., 2003, 2005). Results show that the pressure perturbation has a long reach, while the injected water is confined within a few meters around the injection well. Figures 4c-d show the results for the case of a permeability $5 \cdot 10^{-20}$ m^2: while the pressure front can be up to 8 m away, the injected fluid is confined around the injection point. A larger (smaller) permeability results in larger (smaller) reach of the injected fluid. Simulating permeability varying as a function of elastic or tensile opening of fracture results in a much larger reach as soon as the pressure is increased above the leakage threshold (Zappone et al., 2018). However, this condition was considered a worst-case scenario, as the CS-D experiments aims at injecting at a pressure below the FOP.

Results of the preliminary modelling suggested that a fluid monitoring borehole needed to be placed at the minimum distance allowed by the setup (i.e. 2 m inter-distance at gallery floor). All the different scenario results with fixed permeability and stress-dependent permeability are provided in the Supplementary material (S1 and S2, respectively).

3.2 Boreholes geometry

Due to the considerable anisotropy of seismic (e.g. Nicollin et al. 2008; anisotropy=28%) and electrical (e.g. Nicollin et al. 2010; anisotropy=85%) properties of Opalinus clay, the geophysical monitoring boreholes were oriented in a way that would facilitate the data processing. For this reason, they are oriented such that the 2-D tomographic planes in between these boreholes are normal to the bedding planes (anisotropy symmetry axis within tomography planes). Three geophysical boreholes were drilled with an inclination of 48-51° from vertical to have a perpendicular intersection with the fault and bedding. In addition, the intervals in the injection borehole needed to be in the vicinity of the field of view of the geophysical arrays.

A total of seven boreholes, four vertical (BCS-D1, -D2, -D6, and -D7) and three inclined (BCS-D3, -D4, and -D5), were drilled and equipped in order to perform and monitor a long-term (twelve months) injection of CO_2-saturated water in the fault, to monitor the movement of the water in the fault by geophysical methods and by sampling of fluids. The geometrical layout of the boreholes is illustrated in Fig. 5. Table 1 gives specifications on borehole purpose, diameter, length and orientation.

The boreholes BCS-D3 to -D6 were drilled for specific geophysical investigations. BCS-D3 and -D4 were drilled coplanar to each other, such that they create a plane that intersects the fault zone at a distance of 2 m from the injection intervals. BCS-D5 was drilled on the opposite side of the injection borehole and is also coplanar to BCS-D3. This allows for an additional tomography plane across the injection zone. BCS-D6 is drilled vertical at a distance of 3 meters form BCS-D7 with the purpose of placing sensors for continuous seismic monitoring for better locating seismic events in 3-D.

3.3 Instrumentation

3.3.1 Injection system

The injection system is designed to perform injection separately at four depth intervals in the fault zone. An injection module (Fig. 6) designed for injection over long periods was connected to the borehole BCS-D1. The injection is carried out using a syringe pump (Teledyne ISCO 500D), that is remotely controlled through a dedicated software (DCAM) developed by Solexperts AG. The pump allows the injection of moderate volumes of fluids, with an injection chamber volume of 0.5 l, refill breaks of 2.5 min, and has an accurate control of injection rate from 0.001 to 200 ml/min. The pump is connected to a 10 l tank, where the injection water is pressurized at about 2 MPa and mixed with carbon dioxide (CO_2) and Krypton (Kr) by bubbling. The pressure in the mixing tank is sustained by a pressure regulator mounted on the CO_2 bottle. A circulation pump and a flow meter enable controlled mixing. To resemble the natural composition of formation water, we inject Pearson water A1 type (Marceau et al., 2016), depleted of Mg and Ca, to avoid mineral precipitation and consequent clogging of the lines. Kr is added to the mixture as tracer because it is not present in the formation water and is not reactive. The pressure of CO_2 in the mixing tank is continuously monitored, and the CO_2 content in the injection water is calculated on the basis of the CO_2 dissolution in saline water, at the pressure and temperature conditions of the mixing tank and given the salinity of the Pearson water. The injection module is designed for permanent and remote-controlled injections.

3.3.2 Boreholes instrumentation

Borehole BCS-D1, the injection borehole, and BCS-D2, the fluid-monitoring borehole were equipped with a 4-fold and 6-fold packer system, respectively. Figure 9a displays a schematic layout of the packer system showing packer and interval depths and the intersection with the fault, as from borehole logging.

Pressure at each injection and monitoring interval is monitored with sensors connected at the surface; flow lines and packer lines are realized in stainless steel to avoid corrosion from CO_2 exposure.

Deformation is monitored through Distributed Strain Sensing (DSS) fiber optic (FO) cables, integrated in the packer system, and anchored at each interval to avoid effect of packer inflation on strain measurement. The multiple packers system allows for multiple injection/monitoring intervals, both in the fault zone and in the host rock. All the intervals were saturated with Pearson water A1 type (Marceau et al., 2016), depleted from Mg and Ca, to avoid mineral precipitation.

Boreholes BCS-D3 to 6 were all cased with PVC tubes to assure impermeability of the inner chamber and instrumented with DSS FO cables fixed to the casing to allow distributed deformation measurements. After installation, the annulus between the PVC casing and the borehole wall was grouted with a mixture of bentonite and cement. In order to prevent any possible leakage of CO_2 at the surface of the niche through the monitoring wells, epoxy resin was injected between PVC and borehole wall at a depth below the EDZ and above the fault.

The fiber optic strain sensing cables, 3.2 mm in diameter, are flexible cables, armoured with a central metal tube surrounded by a structured PA outer sheath, containing one single optical fiber (BRUsens strain sensing cables). They are designed to measure a strain range up to 1% (10000 μstrain). Axial deformation is also measured with a chain potentiometer grouted outside the PVC casing in borehole BCS-D5, including 12 measuring sections, ten of which are crossing the fault with 0.5 m inter-distance between each element. The chain potentiometer consists of anchor-elements connected to each other by PVC tubes. The anchors measure unidirectional displacements relative to each other. Standard potentiometric displacement sensors with a measuring range of 100 mm are used for the measurements in the chain.

Fifty ring-shaped stainless-steel electrodes, with an interspacing of 0.5 m, were clamped to the casing in BCS-D3 and 4, to allow electrical resistivity tomography and time-lapse observations on a 2-D plane between the two boreholes. Inside the casing of BCS-D3 a 3-component geophone array of twenty-four geophones (100 Hz) with interspacing of 0.5 m was installed, while identical single 3-component geophones were installed at the bottom of boreholes BCS-D4 to 6. The 3-component geophones were custom-designed by Omniquest Int. and are identical to those installed in a previous MTRL experiment (Manukyan and Maurer, 2018). Eight piezo-sensor elements for high frequency seismic detections were installed in boreholes BCS-D5 and 6 (four each). We used piezoelectric sensors (type GMuG MA-Bls-7-70) designed by the Gesellschaft für Materialprüfung und Geophysik (GMuG). These sensors are similar to those commonly used in laboratory acoustic emission experiments (e.g., Ishida, 2001) and are highly sensitive in the frequency range of 1–100 kHz, with the highest sensitivity at 70 kHz.

As seismic sources, a P- and S-wave sparker is employed in the water-filled PVC-casings of borehole BCS-D4 and BCS-D5 (in D5 for baseline and optionally after the injection experiment). Both these boreholes are in-plane with borehole BCS-D3, thus enabling 2D tomography within the two corresponding planes in relatively high resolution.

3.3.3 Seismic instrumentation in the niche 8

To complete the seismic monitoring network (active and passive), thirty-three one-component geophones (Geospace Corp Corp. Texas) were coupled to the rock behind the shotcrete in the niche. An additional network of 18 piezo-sensors (Type GMuG Ma-BSL-7-70 sensitivity between 1 and 100 kHz) were set up at the surface (clamped to the niche floor), in two parallel lines along the tunnel walls. The sensor spacing is about 2 m. As the piezo-sensors do not have a well-defined instrument response due to resonance peaks that depend upon sensor design and local installation to the rock (Kwiatek et al., 2011), we combined one piezo-sensor with a calibrated one-component accelerometer (type Wilcoxon 736T) that has a flat instrument response in the range 2–17 kHz. The surface instrumentation also comprises six hammer sources installed in a parallel line along the tunnel wall and are within the plane between BCS-D3 and D4.

3.3.4 Fluid sampling and dissolved gas analysis

Two circulation modules were installed for fluid sampling in the intervals of the 6-fold packer system in borehole BCS-D2. The first circulation loop is connected to a gear pump with a flow meter that allows fluid circulation in one selected interval from which fluid samples can be extracted and collected in stainless steel vials maintaining in situ pressure conditions, and therefore avoiding degassing. The circulation guarantees chemical homogeneity in the interval. An EC probe (Hamilton Conducell, 1 – 300 mS/cm) and a pH probe (Hamilton Polilyte Plus, pH range 0-14) are also connected to the flow-through cell. Fluid major element compositions are determined using ion chromatography. Carbon isotopes in dissolved inorganic carbon are determined by isotope ratio mass spectrometry after acidification of the sample to pH < 2 to quantitatively extract the inorganic carbon as CO_2 with an analytical reproducibility better than 0.2 ‰.

A second circulation loop (Fig. 7) allows for *in-situ* analysis of dissolved gas in the fluids in a selected interval. The measurements are performed with a portable mass spectrometer called "miniRuedi" (Brennwald et al., 2016; , Gasometrix GmbH, Switzerland) that allows quantification of He, Ar, Kr, N_2, O_2, and CO_2 partial pressures ratios with a relative analytical uncertainty of about 3%. In addition to monitoring CO_2, we aim at tracking the restitution of Kr that is used as artificial conservative tracer. In this perspective, both conservative and reactive transport processes will be quantified and discussed. We also focus our attention on the evolution of natural dissolved noble gases such as dissolved He and Ar that might reveal mixing with in-situ remobilized fluid (Roques et al., 2020).

3.3.5 Pressure/Displacements/Water Resistivity monitoring in boreholes CS-D7

The CS-D experiment uses a new prototype of the SIMFIP hydromechanical borehole probe (Guglielmi et al., 2013). This new SIMFIP prototype, developed at the Lawrence Berkeley National Laboratory, has been designed for long-term borehole monitoring of micrometre fault zones displacements and eventual associated CO_2 leakage. Main prototype development concerned the possibility for a SIMFIP probe to isolate a long borehole interval including an entire fault zone thickness that would have been identified from an initial borehole logging program.. The MTRL, its Main Fault and the CSD project are the perfect site to test this new prototype at the relevant field scale.

In order to monitor the hydromechanical behaviour of the entire fault zone, a 6.3 m long SIMFIP interval has been designed, and sealed by two 0.9 m long inflatable packers. In this configuration, the SIMFIP sensor is measuring the relative displacement of the upper packer, the lower packer considered fixed. The packers play two roles, sealing the interval to isolate fault zone pore pressure variations and anchoring the SIMFIP sensor to measure the displacement of the fault hanging-wall relative to the foot-wall. A compass set above the upper packer allows orienting the displacement measurements. The SIMFIP sensor is a 0.49 m long and 0.1 m diameter pre-calibrated aluminium cage set on the tube connecting the two packers. When the fault straddled by the packers' interval is deforming, the cage allows obtaining angle dependent strain measurements which can be

used to constrain the full three-dimensional displacement tensor and the three rotations of the upper packer relative to the lower packer.

Borehole pressures are monitored below the lower packer, between the packers and above the upper packer. Water resistivity electrodes have been distributed every 5.54 cm along the entire length of the SIMFIP chamber in order to localize where leaks would possibly occur from the fault zone into the borehole. It was assumed that for example dissolved CO_2 leak would slightly change the formation water resistivity, enough to be detected by the resistivity probe. After several months of tests and monitoring, measurement sensitivities are of 10^{-6} m for displacements and 10^{-3} Pa for pore pressure (Paragraph 4.4). A remote control allows programming the SIMFIP, and for example vary the sampling rate from 1 Hz to 1 kHz depending on the testing protocol.

4. Results from Phase 1

4. 1 Main Fault geometry from cores and logs

All boreholes were cored with exception of BCS-D4. Cores were recovered with a double barrel technique, with the exception of D1 were the Main fault section has been cored with a triple barrel technique. Core recovery was higher than 90%. The boreholes were logged with an oriented optical borehole televiewer, total count natural gamma ray, dual induction, and calliper (four arms in vertical single arm in inclined boreholes). A cross-analysis of the cores and of the logs allowed an accurate reconstruction of the oriented geological log for each borehole. The position of the instrumentation in injection and fluid monitoring boreholes was then decided, based on the fault depth.

The bedding is uniform on both sides of the fault with a mean orientation striking N053 ° and a dip of 46° SE. A top and a base plane, both clearly identified on cores and image logs (Fig. 8a, b), spaced c.a. 1.5 to 3 m, define the Main Fault. In the core there is a sharp discontinuity between undeformed bedding and highly deformed scaly clay material, that consists of a tangled web of slickensides, bounding largely unaltered microlithons (Jaeggi et al., 2017), and is also visible in the image logs. Table 2 displays the depth and orientation of the top and bottom of the Main Fault in all boreholes from image logs analysis. The top and bottom of the Main Fault plane within our study area are variable, with typical strike oriented N031-068° and dipping 56-65°SE. In borehole BCS-D5, the top of the fault has a very steep dip, which is near vertical or perhaps overturned. The fault material between these two planes is heterogeneous, including zones with fault gouge, C'-type shear bands, meso-scale folds, microfolds, numerous fault planes, apparently undisturbed parts and a 'scaly' fabric where the rock splits progressively into smaller fish-like flakes. Moreover, sparse and discontinuous secondary fault planes have been observed above and below the Main Fault.

There are numerous fractures and faults within the Main Fault. The location of the injection (BCS-D1) and monitoring (BCS-D2) intervals within the Main Fault are depicted in Fig. 8c. Within the injection borehole there are fractures with an orientation

similar to the Main Fault, as well as a set with a conjugate orientation (Fig. 8b, d). Borehole injection tests revealed a pressure response in monitoring interval M1 and M2 (see nomenclature of intervals in Fig. 8c) when injecting from injection interval Q4. As such, the structures within these intervals are highlighted in Fig. 8d. While we do observe northward dipping fractures that might connected the Q4 and M1/M2 intervals in other parts of the borehole, these fractures are not directly observed in these intervals.

Core pieces longer than 10 cm were sampled and sealed after undergoing an on-site quality control (i.e., no open fractures, no drilling-induced features, etc.). Samples were wrapped in barrier foil aluminium laminate and vacuum-sealed to limit contact with air. Samples were labelled with respect to the borehole name and order number. For samples that contain fault zone or carbonate lenses, this property is also written beside the sample name on the label. After sealing and labelling samples were stored in a wooden box and shipped to ETH Zurich. Studies on multi-flow transport in fractured rock and geomechanical characterization of the fault and host rock from the CS-D site have been developed in laboratories respectively at Imperial College London and ETH, and at EPFL (Wenning et al., 2019a, b; Minardi et al., 2020).

4.2 Hydraulic characterization

We performed several injection tests to estimate hydraulic properties and opening pressure (FOP) of the fault zone. These tests were essential to identify which intervals would be best candidates for injection and monitoring. Injection always occurred in intervals of the BCS-D1 borehole. The different tests are reported in Table 3 and include:

- Long step test at constant head with 28-30 hours inter-step time (LST).
- Short step test at constant head with 5-10 minutes inter-step time (SST).
- High pressure short step up test at constant head with 5-10 minutes inter-step time (HP-SST); these tests were usually performed after a LST.
- Pulse step test with pump stopped after reaching desired pressure then 10 minutes decay before new step (PST).

While we carried out the tests in several intervals (Q1, Q2, Q4), we performed the analysis only on interval Q4, which is the shallowest interval in the injection borehole (BCS-D1), and which is the one finally chosen for the CO_2-saturated water injection in Phase 2. Our tests gave first order estimates of the initial transmissivity of the fault zone from this interval. Figure 9 shows the results of a LST in interval Q4: only when injecting in this interval we observed a hydraulic response in the fluid monitoring borehole (BCS-D2). This was a critical information to decide the injection interval for the Phase 2 injection. Figure 5a (insert) and 9a show a schematic (plane view) of the distance between the interval Q4 and two monitoring intervals (M1 and M5). Quite interestingly, when injecting in Q4, only the bottom intervals of the fluid monitoring boreholes show pressure variation (e.g., M1 less than 0.1 MPa, Fig. 9b, red curve), while all the others show no variation (e.g., M5, Fig. 9b, green curve). We note that the flow rate never reaches steady conditions for all the steps performed in the analysed test (Fig. 9c).

The transmissivity of the fault zone was estimated by analysing a pulse test (also performed in interval Q4) with a Cooper-Bredehoeft-Papadopulos-Neuzil model (Cooper at al., 1967; Neuzil, 1982; Renard, 2017). Figure 10a-b show the pressure variation and the comparison with the model that results in a transmissivity of 1.8×10^{-13} m^2/s. In the model, the pressure decay is normalized to the peak, and both pressure variation and its derivative are used to estimate transmissivity. We discarded the first 30 seconds of data as these could be influenced by interval storage. For this model, the compressibility of the system was estimated given the injected volume to reach the peak pressure (1.7 MPa). A similar value of transmissivity (2.8×10^{-13} m^2/s) is obtained by analysing the first step of the LST (Fig. 10c-d) with a Jacob and Lohman model (Renard, 2017). For this model, only the flow rate is used to estimate the transmissivity. As above, we discarded the first seconds of data as these are strongly affected by the interval volume and near-borehole skin effects.

4.3 Fault opening pressure

The fault opening pressure (FOP) in the interval Q4 was determined prior to starting the long-term injection with CO_2-saturated water in Phase 2. During the PST-test, the pressure was increased in steps of 0.3 MPa and shut-in after reaching the desired pressure. Figure 11a shows the pressure recorded at injection interval (BCS-D1-Q4). Figure 11b shows an enlargement of the recorded pressure when the pressure drop was more consistent. Figure 11c shows the pressure difference after 10 minutes waiting time compared to the injection pressure. The pressure response is non-linear when injection pressure was raised above 4.5 MPa. The large steps (0.3 MPa) employed do not allow for a precise measure of the FOP, but we can conclude than it is in the range 4.5-4.8 MPa. We performed this test only in the injection interval Q4 because it was the only interval showing pressure response in the monitoring borehole. After reaching this "reactivation", we started the long-term CO_2-saturated fluid injection below the FOP at a constant pressure of 4.5 MPa. An analysis of the decay curve from 4.8 MPa with a Cooper-Neuzil model (Renard, 2017) results in an estimated transmissivity of 9.2×10^{-12} m^2/s, which is more than one order magnitude larger compared to previous estimates (see above). It is worth noting that for the estimate, here we considered only the last step and analysed the decay from considering the previous step pressure (i.e. from 4.8 to 4.5 MPa).

4.4 Borehole stability monitoring in BCS-D7

The SIMFIP probe was installed in the borehole immediately after drilling on October 2018. Figure 12a shows the location of the probe across the fault zone. The installation phase was followed by a period of tuning the packers' pressure until December 19th. Figure 12b-d shows the results of the first 5 months monitoring period, with the packer testing phase highlighted by the red shaded area. The main issue was to maintain the packer pressure constant. For example, during November 2018, packers exhibited a slow deflation that required several manual re-inflations. The problem was fixed in late December 2018 by installing an automatic control of the packer pressure. The four periods of packer pressure variations on January 10th, January 16th, February 1st and March 27th correspond to complementary, manual adjustments of the packer system. This probe is

equipped with sliding-end packers in order to ensure an optimal sealing of the isolated interval. The dimension of the interval evolves in response to the pressure variation and to the consequent deformation of the clay walls. The control of the packers response is therefore crucial. Because the packers slide while their pressure is varying, the chamber pressure and the displacement measurements (since the SIMFIP is anchored with the packers – Fig. 11d) also vary. The packers pressure increase is inducing a chamber pressure decrease, a SIMFIP vertical extension (positive Dz variation) and an equal radial displacement (EW = -NS, see for example February 2019 – Fig. 12d). This response matches with laboratory calibrations, and thus any deviation from them observed in the field might highlight a true hydromechanical evolution of the formation.

Interestingly, the chamber pressure increased by 0.2 MPa during the first month after installation. This period (red shaded area in Fig. 11b-d) could be interpreted as a stress relaxation after borehole drilling. Then, from early December to February, pressure decreased, indicating a potential coupled hydromechanical relaxation (orange shaded area in Fig. 11b-d). Finally, in February 2019 the pressure in the SIMFIP stabilized at about the initial pressurization (~0.3 MPa) (green shaded area in Fig. 11b-d). These long-term pressure variations are not clearly related to packers' effect (although the influence of the packers is observed over shorter periods). Both variations thus relate to the complex borehole pressure equilibration with formation pressure, which occurred in about 5 months. Displacement variations followed these long-term pressure variations. Displacement amplitudes are from 0.3 to 1 mm, the norm of the displacement vector being estimated at 0.95 mm in March 2019after 5 months of monitoring (more than 70% of the displacement occurred after about 1.5 months). These values are in reasonable accordance with strain relaxation effects associated to borehole or gallery excavation observed in other Mt-Terri experiments (Amann et al., 2017). The SIMFIP data exhibit displacement variations in all the three EW, NS and Z directions, thus highlighting the three-dimensional characteristics of such relaxation effects.

The pressure in the interval, pressure in the packer, and displacement have been overall constant since then, with some gaps due to on-site operation in April 2019 (grey shaded area in Fig. 11b-d). Starting from April 2019, the effect of a nearby tunnel excavation is visible on the probe, up to a maximum displacement of about 0.2 mm (Rinaldi et al., 2020).

The accuracy of the SIMFIP is shown in detail in Fig. 12e and 12f. The figures refer to data taken during the LST test, in the same time window shown in Fig 9. The relative and detrended displacement is measured with a delta of about 1 μm (Fig. 12e); after a more accurate calibration of the packer pressure, the delta is reduced to less than 0.5 μm (Fig. 12f).

4.5 Seismic characterization

Active seismic baseline measurements were conducted in January 2019, before the first injection test. They were repeated on June 11th, 2019, before the start of the long-term injection. These baseline measurements were performed with hammer sources applied on the gallery floor and with a seismic sparker source employed in borehole BCS-D4 and -D5, while all geophones and piezo-electric transducers installed in boreholes and in the gallery were recording. Example data are shown in Fig. 13. They have been recorded with a geophone cemented in borehole BCS-D3, while the sparker source was fired in 25 cm intervals

in borehole BCS-D4. It shows a clear P-wave arrival (A), which is slightly delayed for sources fired within the Main Fault (B). Additionally, slow- and fast S-wave modes can be identified (C) and strong linear events, which are caused by tube waves propagating along the source borehole (D) and are reflected at the Main Fault (F).

The data shown in Fig. 13 have been processed using the following processing steps:

- median filter (subtraction of median amplitude of entire trace, removing a constant shift from the signal);
- bandpass filter;
- zero-time correction by cross-correlation of recorded trigger signals;
- trace stacking of 5-10 repeated shots.

For characterizing the seismic P-wave velocity (V_P) structure in the region of the CS-D experiment, 2-dimensional P-wave travel time tomography was carried out within planes between boreholes BCS-D3 and -D4 as well as between boreholes BCS-D3 and -D5. Here we show the tomogram measured with a P-wave sparker source from borehole BCS-D4 and with the cemented geophone array in borehole BCS-D3. The tomographic imaging involved the following procedure:

- automatic picking of first arrival times;
- picking refinement with cross-correlation (e.g. Schopper et al., 2020);
- anisotropy correction;
- iterative travel time inversion (after Lanz et al., 1998).

The clay bedding, along which the V_p attains maximum values, is oriented normal to the tomographic planes. Therefore, it was assumed that no off-plane effects occur due to the V_P anisotropy. Anisotropic effects within the tomographic plane were minimized by normalizing the travel times. This travel time normalization is displayed in Fig. 14, where prior to normalization (a) V_P along the bedding plane reaches values of approximately 2870 m/s and extrapolating to angles normal to the bedding planes yields $V_P \approx 2280$ (Fig. 14a). This leads to an overall V_P-anisotropy coefficient $A = (VP,max–VP,min)/VP,min = 0.26$. After normalization of travel times, normalized P-wave velocities $V_{P,n}$ are around 2580 m/s in average (Fig. 14-b).

In Fig. 15, the resulting $V_{P,n}$ tomogram between borehole BCS-D3 and D4 is shown. It was computed with the baseline-data recorded on June 11th, 2019. The inverted V_P-model explains the observed travel times with an average RMS error of 0.05 ms. The velocity values of the tomogram are displayed as normalized values according to Fig. 14, which means that they are average values of the in fact anisotropic velocities. The location of the Main Fault, estimated by interpolating observations from all CS-D boreholes (Fig. 4a), is displayed by the thin black lines. The Main Fault is causing a clear low-velocity zone in the V_P-tomogram, which can be clearly identified by cross-hole seismic. Furthermore, V_P appears to be larger in the footwall than in the hanging wall. Heterogeneities within these two units were most probably due to our assumption that the anisotropy is homogeneous, whereas in fact the anisotropy is slightly higher in the footwall than in the hanging wall as shown in Fig. 14a.

5. Discussion

Although focusing on the characterization of the reservoir and on the development of our experimental setup at the meter scale, the initial results presented in this contribution already provide important insights for our understanding of the processes involved in large scale CO_2 storage operations.

The structural mapping during drilling allowed to adjust the boreholes position and to install the packers in the injection, the monitoring systems, and the SIMFIP boreholes to span the entire thickness of the fault zone. Core mapping and borehole optical televiewer logs clearly identify the Main Fault in the host Opalinus Clay , marked by cm-thick dark fault gouge and scaly clay texture (Jaeggi et al., 2017) . The contact between fault and host rock is sharp (Fig. 8a). The Main Fault in the vicinity of the CS-D experiment is between 1 to 3 m thick with typical strike oriented N031-068° and dipping 56-65°SE. The upper contact, marked by the ~ 1 cm thick gouge layer followed by a ~ 10 to 20 cm thick scaly clay, is similar to the upper fault contact in Gallery 98 (Jaeggi et al., 2017) and the faults observed in the FS-B boreholes (Guglielmi et al., 2020a). A layer of scaly clay also marks the bottom of the main fault. These trends show the strike parallel similarities that span across the > 50 m in the rock laboratory. While the tops and bottoms have similar orientations to the Main Fault in the gallery and other boreholes (Nussbaum et al., 2011, Jaeggi et al., 2017, Guglielmi et al., 2020), the internal structure is very heterogeneous. The majority of fractures within the Main Fault have a similar trend to the boundaries (cf. Jaeggi et al., 2017). However, several conjugate structures and fractures do not fall within the Main Fault trend. These fractures correspond to S-C and Riedel R- and P- structures (Nussbaum et al., 2011). The heterogeneity of structural fabrics within the fault core that characterize the Main Fault is a common feature of faults in clay and makes it difficult to determine the hydraulic properties of such faults. The internal architecture of a fault in clay, similar in scale to the Main Fault at MTRL, has been described at the Tournemire underground lab in France (Dick et al., 2016, and references therein). In this case a fault core has been distinguished from a damaged zone; the core comprises a gouge with thin dark cm-thick bands, cataclasites, rock portions with folded foliation planes, and lenses of less deformed rock, all elements similar to the Main Fault at MTRL. The damage zones is represented by a dense network of small faults, fractures, and calcite veins, that extends 2-3 m from the fault core. Pulse tests in Tournemire revealed hydraulic conductivity along the core-damage zone boundary one-two orders of magnitude greater the than in the undisturbed rock (Dick et al., 2016). Marschall et al. (2005) investigated hydraulically sections of the fault zone at MTRL, and showed that the permeability of faulted Opalinus Clay and of undisturbed rock is not significantly different.

During Phase I, several injection tests were performed to characterize the hydraulic response of the site and to determine if there was any hydraulic response between the injection and monitoring boreholes. An important first result of the CS-D experiment is that the injected fluid is channelled along preferential pathways rather than along the fault plane, although the transmissivity of these pathways remains extremely low (order of 10^{-13} m^2/s). During the hydraulic tests, a clear pressure response was observed in the monitoring borehole (BCS-D2, intervals M1, M2) when injection occurred in the uppermost interval of the injection borehole (BCS-D1, interval Q4). If this observation was linked to poroelastic effects, we would expect

a similar pressure increase in all interval at approximately the same distance, although the heterogeneity of the medium might generate some differences. As the pressure variation in the monitor borehole is only observed in the bottom intervals, we argue that the poroelastic response is negligible, and that the flow follows complex pathways within the fault. A pronounced fracture possibly connecting injection and monitoring boreholes in the direction Q4-M1 was not identified in these specific intervals, but conjugate structures (NW dipping fractures, Fig. 8b, d) could explain the fluid pressure connection of the Q4 injection interval to the M1 and M2 monitoring intervals.

Fault transmissivity models assume that the system is a homogeneous porous medium, with radial flow from the borehole. However, it should be noted that the Main Fault may behave rather as a fractured system, given the interconnection of specific intervals, rather than yielding a uniform/homogeneous response. In other words, our estimate relies on the assumption of a homogeneous representation of the rock with effective hydraulic properties, which might fail in capturing the real pressure distribution in such a fractured environment. Nevertheless, the transmissivity estimates agree with previous tests conducted in boreholes reaching the fault in shaly-facies at ca. 9 m depth from another niche (Marschall et al., 2005) and could indicate a permeability in the fault zone in the order of 10^{-20} m^2, when assuming a layer as thick as the injection interval (1.4 m). An analysis of all other tests and decay curve results in similar value for the transmissivity.

The estimated permeability is extremely low, and extrapolating this value to full-scale injection plants would not results in major CO_2 leakage if constant through the operational phase. Indeed, such a low value makes the fault as impermeable as the caprock itself, but changes in permeability and/or porosity due to geochemical/geomechanical process could in the long term affect the sealing capacity, albeit in a more heterogeneous way compared to what expected during planning phase of the experiment.

An additional injection test was designed to determine the fault opening pressure (FOP), i.e. the pressure at which the fractures are jacked opened and allow leakage. By performing a series of step tests, the FOP occurred in the range 4.5 to 4.8 MPa. This value is in agreement with previous studies at Mont Terri (e.g. 5.4 MPa – Guglielmi et al., 2020a). While the recorded signal at the injection point clearly indicated a fracture reactivation, and the estimated transmissivity increased by one order of magnitude, the pressure response was not clear at the monitoring point. It should be noted however that the FOP test (PST3 – Table 3) was performed right after an important excavation that occurred in a tunnel nearby (Rinaldi et al., 2020), which could have affected the local state of stress, thus allowing for opening of fractures/cracks at lower pressure.

The reactivation of a fracture resulted in a stronger pressure decay compared to previous steps, although no obvious deformation was recorded at either the SIMFIP, or the potentiometer chain, or the fiber optic. It is then difficult to estimate the orientation of the reactivated fracture(s) by looking at the injection data alone. Some minor deformations were observed in the potentiometer chain during previous tests in the period March/April 2019 (see supplementary figure S3), but it is hard to discriminate the small effect of injection from other processes occurring at depth in the long term, such as borehole stabilization

or stress relaxation after excavation. For example, the SIMFIP probe, placed at about 7 m from the injection point and being able to capture submicron deformation, should be able to record some signals. However, data exhibit complex three-dimensional strain relaxation effects that lasted about 1.5 months after drilling. These effects with deformations in the order of microns are affecting the boreholes' interval fluid pressures in and outside the fault zone, and may mask any effect linked to the injection. Such a "long" relaxation period is consistent with observations made in other Mt Terri experiments dedicated to the long-term hydromechanical behaviour of the excavation damage zone around galleries or boreholes in low permeable Opalinus Clay (Bossard et al., 2017). How permanent and how amplified are these effects in the fault zone will inform on the evolution of the damage zone in the near field of boreholes drilled through faulted caprocks.

From the active seismic baseline data recorded during Phase I, we analysed the P-wave velocity (V_P) anisotropy. V_P-values averaged over the entire rock volume including the Main Fault were observed to be around 2870 m/s in the direction of the clay bedding in the host rock, and around 2280 m/s normal to the clay bedding. 2-dimensional tomographic imaging was carried out using anisotropy-normalized P-wave travel times. The resulting tomogram was capable of clearly revealing the location of the Main Fault in the form of a pronounced low-velocity zone correlating well with direct borehole observations. Values of V_P we observed in situ are clearly smaller than what has been previously measured by other researchers on drill cores in the laboratory (e.g. Bossart et al. (2017), 2220-3020 m/s normal to bedding, 3170-3650 m/s parallel to bedding), but exhibit a similar degree of anisotropy, with A = 0.26, which is close to A = 0.3 estimated after Bossart et al. (2017). Lower values in absolute V_P compared to ultrasonic measurements have been expected in accordance with the Kramers-Kronig dispersion relation (e.g. Mavko et al., 2009). In situ seismic crosshole measurements have previously been performed by Schuster et al. (2017). For apparent velocities outside the EDZ, they recorded values of around 3100 m/s for ray paths approximately parallel to bedding, and around 2600 m/s for rays normal to bedding. Fitting an ellipse through the apparent velocities (similar to Fig. 14) they estimated an anisotropy coefficient A = 0.20, which is close to our observation. The difference could be due to heterogeneities within the shaly-facies of the Opalinus Clay, but also because in our case ray coverage normal to the bedding was poor, whereas Schuster et al. (2017) did not cover ray paths exactly parallel to bedding. To the best of our knowledge, seismic traveltime tomography across a larger fault in Opalinus Clay hasn't been performed before, but Jaeggi et al. (2017) measured ultrasonic interval velocities along a borehole which is crossing the Main Fault in Mont Terri and is oriented around 40° to the bedding planes. Within Main Fault-sections with scaly clay, they observed distinctly reduced V_P values as low as 2000 m/s. This is even lower than what we observed in Fig. 15, and can be attributed to the higher resolution of the interval velocities which enables to resolve individual sections of scaly clay, whereas with our crosshole measurements we measured V_P of the Main Fault consisting of a mixture of scaly clay and lenses of undisturbed Opalinus Clay.

All the injection tests during the Phase I were also monitored for induced acoustic emissions. Eight piezo sensors installed in boreholes at a distance varying from about 2.5 m to 10 m from injection point (Fig. 5 a,b) were recording at very high sample frequency (0.2 MHz) during all injection tests. Despite reaching elevated pressure (e.g. 6 MPa in test Q4 - HPP-SST – Table 4), and while the pressure response was clear at a distance of about 2.5 m, no signal was recorded by the piezo-sensors. This is not surprising, given the very low tendency of clay rock to generate seismic events (Orellana et al., 2018), but in similar conditions some seismicity was observed at an experiment nearby with resulting much enhanced flow (Guglielmi et al., 2020a). Furthermore, the Opalinus Clay features quite high attenuation of seismic waves, in particular in regions where fractures and cracks exist (Nicollin et al., 2008): hence even for the tests where a clear geomachanical response is observed (FOP test – Fig. 11), the 2.5 m minimum distance between injection point and piezo-sensor could be already enough to damp the high frequency at which the acoustic emission should be observed.

6. Outlook for the long-term injection and implications for large scale storage

Based on the hydraulic observations, the pressure response suggests that the highest probability of possible flow connection exists between injection interval Q4 and monitoring interval M1 and M2. Therefore, the long-term injection began in June 2019 (Phase 2) from the Q4 injection interval in the uppermost part of the fault, with Pearson water saturated with a mixture of CO_2 and Kr at a constant pressure of 4.5 MPa (below the FOP). The injection is as for November 2020 still ongoing.

The long-term injection at CS-D will allow shedding light on the several points listed below.

- The fault transmissivity evolution will be observed over a long period of time (12-18 months). Continuous pressurization might weaken the fault, inducing seismic events or aseismic deformation that could enhance the permeability of the fault. Results from previous experiments (Guglielmi et al., 2020a), data from the CO_2 demonstration site at In Salah, Algeria (Rinaldi et al., 2017; Shi et al., 2013), as well as numerical modelling (Rutqvist et al., 2016) clearly show that this could happen in caprocks. We will observe also possible fault healing mechanisms (swelling of the clay) over a prolonged time.
- While a one-year experiment might not allow capturing all the geochemical processes involved in long-term injection operation, this experimental setup will allow monitoring the breakthrough of a CO_2-rich fluid, and the quantification of mixing with resident fluids over a prolonged period of time, and possibly also the description of the main geochemical interactions between the fluids and the rock.
- Advanced monitoring instrumentation will be tested in the long term. In particular two instruments that strongly enhance the monitoring capabilities are: i) the SIMFIP, a probe capable of measuring three-dimensional deformation of the entire fault zone; ii) the “miniRuedi”, a portable mass-spectrometer that allows for monitoring the possible CO_2 breakthrough at given interval at depth. The highly dense network of instruments will allow to fully characterize the

fluid dynamic at an unprecedented level of details for a fault zone in a caprock. Understanding the dynamic of the system will allow to better understand processes relevant for enabling full scale underground CO_2 storage.

- Geophysical measurements will further strengthen the point above. Given the dense active seismic sensors network, regular survey will allow to monitor for changes in the flow, in particular if the CO_2 separates from the fluid as a gas phase and saturate the fault zone. In addition to seismic measurement, we will perform regular rock electrical resistivity measurements to allow imaging any changes in fluid properties: already the difference between in-situ water and CO_2-saturated synthetic water could create enough contrast in the decameter scale of the experiment. Regular monitoring at CS-D will allow for time-lapse images with detailed spatial and temporal resolution: in this way, we aim at reaching the lowest threshold to detect fluid flow in low permeable formations.
- Finally, the CS-D permanent installation will allow for more than one single test. The CS-D experiment, and its successive series of tests, will produce a considerable amount of data that are essential for a proper calibration of numerical models. With a data-driven approach, they will help to fill the gap between observed changes in rock permeability and modelling.

7. **Conclusions**

In this paper, we describe the setup of the *in-situ* CS-D experiment (Carbon Sequestration - Series D) at the Mont Terry Rock Laboratory. We drilled and instrumented a series of boreholes to perform long-term (one year) experiments and to study sealing and induced seismicity related to leakage through low permeable faulted caprocks. The decameter scale experimental setup allows for close monitoring of fluid injected into a fault zone in the Opalinus Clay, simulating leakage through a faulted caprock at shallow depth. We installed geophysical, hydraulic, geomechanical and geochemical instrumentation that enable monitoring of several of the thermo-hydro-mechanical-chemical processes that occur at reservoir depth. In particular, our monitoring capabilities profited from two innovative instruments, which consist of: i) a probe capable of measuring three-dimensional deformation of the entire fault zone; ii) a portable mass-spectrometer that measures partial pressure of dissolved gases (He, Ar, Kr, CO_2, etc.) in water, thus allowing the detection of the CO_2 breakthrough (i.e. the dissolved CO_2 from the injected CO_2-rich water) at given interval at depth.

We also present here the results of the site characterization (Phase I), which highlights the complexity and uniqueness of the experiment.

Some of the aims of the CS-D experiment listed in section 2.1 could already be achieved in the characterization phase. One of them was to better understand the mobility of CO_2-rich water through the fault. Structural mapping and hydraulic

characterization show that the fluid does not flow preferentially along the fault but it is confined in small regions/fractures crosscutting the fault, even if the estimated permeability is extremely low.

Another aim of the CS-D experiment was to test the occurrence of induced micro-seismicity in clay. No induced seismicity has been detected, even at an injection pressure higher than the Fault Opening Pressure determined in previous experiments. The seismic characterization successfully highlights the fault zone as a region of low velocity anomaly. While the rock samples from the host rock and fault zone exhibit very similar elastic properties (Wenning et al., 2019a), the internal structure of the fault defines a different anisotropy pattern inside the fault juxtaposed to the host rock, thus strongly contributing to the seismic anomaly. Nevertheless the resolution does not allow to image small fractures through which the fluid flow may occur.

Many aims of the CS-D experiment (evolution of permeability after long-term exposure to CO_2, variation of geomechanical response with time) remain to be tackled, and will hopefully be achieved through the analysis of the data obtained during the second phase, i.e. the long-term injection of CO_2 saturated water.

Code and Data availability

Codes for numerical modelling are copyright of the LBNL. Code for analysis of injection tests are available at: https://github.com/UniNE-CHYN/hytool. All data analysed in this paper are available under request from alba.zappone@sed.ethz.ch.

Sample availability

Core samples could be obtained by submitting a proposal for experiment at claudio.madonna@erdw.ethz.ch.

Acknowledgements

The CS-D experiment is part of the ACT ELEGANCY, Project No 271498. ELEGANCY has received funding from DETEC (CH), BMWi (DE), RVO (NL), Gassnova (NO), BEIS (UK), Gassco, Equinor and Total, and is co-funded by the European Commission under the Horizon 2020 programme, ACT Grant Agreement No 691712. This project is supported by the Pilot and Demonstration Programme of the Swiss Federal Office of Energy (SFOE).

CS-D is co-funded by the swisstopo, Chevron, Total, and receives in-kind contribution from the Lawrence Berkeley National Laboratory.

We are thankful to swisstopo, and in particular to Paul Bossart, David Jaeggi, Senecio Schefer, Thierry Theurillat and the Mont Terri rock laboratory team for onsite support. We thank Prof. Hans-Ruedi Maurer, from Earth Science Department in ETH Zurich, for productive and cooperative discussions on data analysis. We are grateful to Ulrich W. Weber from University of Uppsala, for providing support for dissolved gas monitoring, and for data discussion. We thank Demir Semih Baris, Madalina Jaggi, Maria Kakurina, Nils Knornschild, Marija Lukovic, Linus Villiger, Thomas Mörgeli, Michelle Robertson and Chet Hopp for technical support, scientific advice, and/or on-site assistance.

Key contractors of the CS-D experiment are:

- GeoSonic France, for the drilling of the boreholes
- Solexperts Switzerland, for the design, installation, operation and maintenance of the injection equipment
- Terratec Germany, for borehole logging.

References

Aagaard, B. K., Skurtveit E., Wangen, M.: Critical Factors for Considering CO_2 Injectivity in Saline Aquifers , FME SUCCESS Synthesis report Volume 3, Rohaldin Miri and Helge Hellevang Eds, pp. 24, 2018.

Alemu, B. L., Aagaard, P., Munz, I. A., and Skurtveit, E.: Caprock interaction with CO_2: A laboratory study of reactivity of shale with supercritical CO_2 and brine, Applied Geochemistry, 26, 1975–1989, 2011.

Al Hosni, M., Vialle, S., Gurevich, B., and Daley, T. M.: Estimation of rock frame weakening using time-lapse crosswell: The Frio brine pilot project, Geophysics, 81, B235–B245, 2016.

Amann, F., Wild, K. M., Loew, S., Yong, S., Thoeny, R., and Frank, E.: Geomechanical behaviour of Opalinus Clay at multiple scales: results from Mont Terri rock laboratory (Switzerland), Swiss Journal of Geosciences, 110 (1), 151–171, 2017.

Blaesi, H. R., Moeri, A., and Bossart, P.: Results of the Phase 1 drilling campaign, Mont Terri Technical Report, TR96-01, Federal Office of Topography (swisstopo), Wabern, Switzerland, 1996.

Bossart, P., Bernier, F., Birkholzer, J., Bruggeman, C., Connolly, P., Dewonck, S., Fukaya, M., Herfort, M., Jensen, M., Matray, J.-M., Mayor, J. C., Moeri, A., Oyama, T., Schuster, K., Shigeta, N., Vietor, T., and Wieczorek, K.: Mont Terri rock laboratory, 20 years of research: introduction, site characteristics and overview of experiments, Swiss Journal of Geosciences, 110(1), 3-22, 2017.

Bossart, P., Meier, P.M., Moeri, A., Trick, T., and Mayor, J.-C.: Geological and hydraulic characterisation of the excavation disturbed zone in the Opalinus Clay of the Mont Terri Rock Laboratory, Engineering Geology, 66 (1–2), 19-38, 2002.

Brennwald, M. S., Schmidt, M., Oser, J., and Kipfer, R. A: Portable and Autonomous Mass Spectrometric System for On-Site Environmental Gas Analysis, Environmental Science & Technology, 50, 13455–13463, 2016.

Busch, A. and Kampman, N.: Migration and Leakage of CO_2 From Deep Geological Storage Sites. In Geological Carbon Storage: Subsurface seals and caprock integrity (eds S. Vialle, J. Ajo-Franklin and J.W. Carey). doi:10.1002/9781119118657.ch14, 2018.

Caine, J. S., Evans, J. P., Forster C. B.: Fault zone architecture and permeability structure. Geology, 24 (11), 1025–1028 doi: https://doi.org/10.1130/0091-7613(1996)024<1025:FZAAPS>2.3.CO;2, 1996.

Cooper, H.H., Bredehoeft, J.D., I.S. Papadopulos I.S.: Response of a finite-diameter well to an instantaneous charge of water Water Resour. Res., 3 (1967), pp. 263-269, 5, 697–700, https://doi.org/10.1002/ghg.1577, 2015.

Cozier, M.: The UN COP21 Climate Change Conference and the role of CCS, Greenhouse Gases: Science and Technology

Credoz, A., Bildstein, O., Jullien, M., Raynal, J., Pétronin, J.-C., Lillo, M., Pozo, C., and Geniaut, G.: Experimental and modeling study of geochemical reactivity between clayey caprocks and CO_2 in geological storage conditions, Energy Procedia, 1, 3445–3452, 2009.

Dick, P., Wittebroodt, C., Courbet, C., Sammaljärvi, J., Estève, I., Matray, J.-M., et al. : The internal architecture and permeability structures of faults in shale formations. The Clay Minerals Society Workshop Lectures Series, 21(17), 227–242, 2016.

Fang, Y., Baojun, B., Dazhen, T., Dunn-Norman, S., and Wronkiewicz, D.: Characteristics of CO_2 sequestration in saline aquifers, Petroleum Science, 7, 83-92, doi:10.1007/s12182-010-0010-3, 2010.

Faulkner, D.R., Jackson, C.A.L., Lunn, R.J., Schlische, R.W., Shipton, Z.K., Wibberley, C.A.J., and Withjack, M.O.: A review of recent developments concerning the structure, mechanics and fluid flow properties of fault zones, Journal of Structural Geology, 32, 1557-1575, doi:10.1016/j.jsg.2010.06.009, 2010.

Feitz, A., Tertyshnikov, K., Pevzner, R., Ricard, L., Harris, B., Schaa, R., Schacht, U., Kalinowski, A., Vialle, S., Glubokovskikh, S., Lebedev, M., Tenthorey, E., Pan, Z., Ennis-King, J., Wang, L., Hossein, S., Ransley, T., Radke, B., Urosevic, M., Singh, R.: The CO2CRC Otway shallow CO_2 controlled release experiment: Preparation for Phase 2, Energy Procedia, 154, 145-150, doi:10.1016/j.egypro.2018.11.024, 2018.

Gemmer, L., Hansen, O., Iding, M., Leary, S. and Ringrose, P.: Geomechanical response to CO_2 injection at Krechba, In Salah, Algeria, First Break, 30(2),79-84, 2012.

Guglielmi, Y., Birkholzer, J., Rutqvist, J., Jeanne P., and Nussbaum C.: Can fault leakage occur before or without reactivation? Results from an in situ fault reactivation experiment at Mont Terri, Energy Procedia, 114, 3167 -3174. Greenhouse Gas Control Technologies 13th International Conference, 14-18 November 2016, Lausanne, Switzerland, 2016.

Guglielmi, Y. , Cappa, F., Lançon, H., Janowczyk, J. B., Rutqvist, J., Tsang C. F., and Wang, J. S. Y.: ISRM Suggested Method for Step-Rate Injection Method for Fracture In-Situ Properties (SIMFIP): Using a 3-Components Borehole Deformation Sensor, in: The ISRM Suggested Methods for Rock Characterization, Testing and Monitoring: 2007-2014, edited by: Ulusay R., Springer, Cham. doi:10.1007/978-3-319-07713-0_14, 2013.

Guglielmi, Y., Nussbaum, C., Robertson, M., Ajo-Franklin, J., Zappone, A., Kloppenburg, A., and Birkholzer, J.: FS-B Experiment: Imaging the long-term loss of faulted host rock integrity - Test plan, Mont Terri Technical Note TN2018-20, 2019.

Guglielmi, Y., Nussbaum, C., Jeanne, P., Rutqvist, J., Cappa, F., and Birkholzer, J.: Complexity of fault rupture and fluid leakage in shale: Insights from a controlled fault activation experiment, Journal of Geophysical Research: Solid Earth, 125, e2019JB017781. doi:10.1029/2019JB017781, 2020a.

Guglielmi, Y., Nussbaum, C., Rutqvist, J., Cappa, F., Jeanne, P., and Birkholzer, J.: Estimating perturbed stress from 3-D borehole displacements induced by fluid injection in fractured or faulted shales, Geophysical Journal International, 221(3), 1684–1695, doi:10.1093/gji/ggaa103, 2020b.

Hangx, S., van der Linden, A., Marcelis, F., and Bauer, A.: The effect of CO_2 on the mechanical properties of the Captain Sandstone: Geological storage of CO_2 at the Goldeneye field (UK), International Journal of Greenhouse Gas Control, 19, 609–619, 2013.

Hostettler, B., Reisdorf, A. G., Jaeggi, D., Deplazes, G., Bläsi, H.-R., Morard, A., Feist-Burkhardt, S., Waltschew, A., Dietze, V., and Menkveld-Gfeller, U.: Litho- and biostratigraphy of the Opalinus Clay and bounding formations in the Mont Terri rock laboratory (Switzerland), Swiss Journal of Geosciences, 110, doi:10.1007/s00015-016-0250-3, 2017.

Hovorka, S. D., Meckel, T. A. and Treviño, R. H.: Monitoring a large-volume injection at Cranfield, Mississippi—Project design and recommendations, International Journal of Greenhouse Gas Control, 18, 345–360, 2013.

IPCC 2005. Carbon Dioxide Capture and Storage. An IPCC Special Report on Carbon Dioxide Capture and Storage. In B. Metz, O. Davidson, H. de Coninck, M. Loos & L. Meyer (Eds), IPCC special report on carbon dioxide capture and storage. Cambridge University Press, Cambridge United Kingdom and New York, NY, USA, 2005.

IPCC 2018. Global warming of 1.5°C. An IPCC Special Report on the impacts of global warming of 1.5°C above pre-industrial levels and related global greenhouse gas emission pathways, in the context of strengthening the global response to the threat of climate change, 2018.

IPCC 2019. Refinement to the 2006 IPCC Guidelines for National Greenhouse Gas Inventories https://www.ipcc.ch/report/2019-refinement-to-the-2006-ipcc-guidelines-for-national-greenhouse-gas-inventories/

Ishida, T.: Acoustic emission monitoring of hydraulic fracturing in laboratory and field, Construction and Building Materials, 15(5–6), 283-295, https://doi.org/10.1016/S0950-0618(00)00077-5, 2001.

Jacob, C. E., and Lohman, S. W: Non-steady flow to a well of constant drawdown in an extensive aquifer, Trans., Am. Geophys. Union, 33, 559–569, 1952.

Jaeggi, D., Laurich, B., Nussbaum, C., Schuster, K., Connolly, P., Tectonic structure of the “Main Fault” in the Opalinus Clay, Mont Terri rock laboratory (Switzerland). Swiss Journal of Geosciences, 110, 67–84, 2017. https://doi.org/10.1007/s00015-016-0243-2

Jha, B. and Juanes, R.: Coupled modeling of multiphase flow and fault poromechanics during geologic CO_2 storage, Energy Procedia, doi:10.1016/j.egypro.2014.11.360, 2014.

Jia, B., Tsau, J.-S., and Barati, R.: A review of the current progress of CO_2 injection EOR and carbon storage in shale oil reservoirs, Fuel, 236, 404-427, ISSN 0016-2361, doi:10.1016/j.fuel.2018.08.103, 2019.

Kampman, N., Busch, A., Bertier, P., Snippe, J., Hangx, S., Pipich, V., Di, Z., Rother, G., Harrington, J. F., Evans, J. P., Maskell, A., Chapman, H. J. and Bickle, M. J.: Observational evidence confirms modelling of the long-term integrity of CO_2-reservoir caprocks, Nature Communications, 7, Article number: 12268, 2016.

Kaszuba, J. P., Janecky, D. R., and Snow, M. G.: Experimental evaluation of mixed fluid reactions between supercritical carbon dioxide and NaCl brine: Relevance to the integrity of a geologic carbon repository, Chemical Geology, 217, 277–293, 2005.

Kwiatek, G., Plenkers, K., Dresen, G., and Group, J. R.: Source pa-rameters of picoseismicity recorded at mponeng deep gold mine,South Africa: implications for scaling relations, B. Seismol.Soc. Am., 101, 2592–2608, https://doi.org/10.1785/0120110094, 2011.

Lanz, E., Maurer, H., and Green, A. G.: Refraction tomography over a buried waste disposal site, Geophysics, 63(4), 1414-1433, 1998.

Le Guen, Y., Renard, F., Hellmann, R., Brosse, E., Collombet, M., Tisserand, D., and Gratier, J.-P.: Enhanced deformation of limestone and sandstone in the presence of high P CO_2 fluids, Journal of Geophysical Research, 112, B05421, 2007.

Manceau, J.C., Tremosa, J., Lerouge, C., Gherardi, F. , Nussbaum, C., Wasch, L.J., Alberic, P. , Audigane, P., Claret, F. , Well integrity assessment by a 1:1 scale wellbore experiment: Exposition to dissolved CO_2 and overcoring, International Journal of Greenhouse Gas Control, 54, 258-271, 2016.

Manukyan, E., and Maurer, H.: Imaging of radioactive waste repository with vertically transversely isotropic full waveform inversion, SEG Technical Program Expanded Abstracts, 4743-4747, 2018.

Marschall, P., Crosisé, J., Schlickenrieder, L., Boisson, J.Y., Vogel, P., Yamamoto, S.: Synthesis of hydrogeological investigations at the Mont Terri site (Phases 1 to 5), Mont Terri Technical Report, TR2001-02. Federal Office of Topography (swisstopo), Wabern, Switzerland, 2003.

Marschall, P., Horseman, S., and Gimmi, T.: Characterisation of gas transport properties of the Opalinus Clay, a potential host rock formation for radioactive waste disposal, Oil & gas science and technology, 60, 121–139, 2005.

Mavko, G., Mukerji, T., and Dvorkin, J.: The Rock Physics Handbook: Tools for Seismic Analysis of Porous Media (2nd Edn.), Cambridge University Press, 2009.

Michael, K., Avijegon, A., Ricard, L., Strand, J., Freifeld, B., Woitt, M., Pervukhina, M., Tertyshnikov, K. , Pevzner, R., Rachakonda, P., Larcher, A., Dance, T., Myers, M., Delle-Piane, C., Feitz, A., Stalker, L., Myers, J., Langhi, L., and Hortle A.: The CSIRO In-Situ Laboratory – a Facility for CO_2 Injection Testing and Monitoring in a Fault Zone; ECCSEL Workshop Underground laboratories for CO_2 Geological Storage Research, 5-6 June 2019, Nancy, France, 2019.

Michael, K., Golab, A., Shulakova, V., Ennis-King, J., Allinson, G., Sharma, S., and Aiken, T.: Geological storage of CO_2 in saline aquifers—A review of the experience from existing storage operations, International Journal of Greenhouse Gas Control, 4(4), 659-667, doi:10.1016/j.ijggc.2009.12.011, 2010.

Mikhaltsevitch, V., Lebedev, M. and Gurevich, B. A.: Laboratory Study of the Elastic and Anelastic Properties of the Sandstone Flooded with Supercritical CO_2 at Seismic Frequencies, Energy Procedia, 63, 4289–4296, 2014.

Minardi, A., Stavropoulou, E., Kim, T., Ferrari, A., Laloui, L.: Experimental assessment of the hydro-mechanical behaviour of a shale caprock during CO_2 injection, International Journal of Gas Control (submitted), 2020.

Myers, M., White, C., Pejcic, B., Feitz, A., Roberts, J., Oh,Y-Y., Xu, L., Ricard, L., Michael, K., Avijegon, A., Rachakonda, P. K., Woltering, M., Larcher, A., Stalker, L., Hortle, A.: CSIRO In-Situ Lab: A multi-pronged approach to surface gas and groundwater monitoring at geological CO2 storage sites, Chemical Geology, 545, 119642,ISSN 0009-2541,https://doi.org/10.1016/j.chemgeo.2020.119642, 2020.

Neuzil, C.E.: On conducting the modified slug test in tight formations, Water Resources Research., 18, 439-441, 1982.

Nicollin, F., Gibert, D., Bossart, P., Nussbaum, C., and Guervilly, C.: Seismic tomography of the excavation damaged zone of the Gallery 04 in the Mont Terri Rock Laboratory, Geophysical Journal International, 172(1), 226-239, 2008.

Nicollin, F., Gibert, D., Lesparre, N., and Nussbaum, C.: Anisotropy of electrical conductivity of the excavation damaged zone in the Mont Terri Underground Rock Laboratory, Geophysical Journal International, 181(1), 303-320, 2010.

Nussbaum, C., Bossart, P., Amann, F., and Aubourg, C.: Analysis of tectonic structures and excavation induced fractures in the Opalinus Clay, Mont Terri underground rock laboratory (Switzerland), Swiss Journal of Geosciences, 104, 187–210, 2011.

Nussbaum, C., Kloppenburg, A., Bossart, P., Caër,T.: Tectonic evolution around the Mont Terri rock laboratory, northwestern Swiss Jura: constraints from kinematic forward modelling, Swiss Journal of Geosciences, 110, 39-66, doi:10.1007/s00015-016-0248-x, 2017.

Orellana, L. F., Scuderi, M. M., Collettini, C. & Violay, M.: Frictional Properties of Opalinus Clay: Implications for Nuclear Waste Storage. J. Geophys. Res. Solid Earth 123, 157–175, DOI: 10.1002/2017JB014931, 2018.Pfiffner, O. A (Eds.): Geology of the Alps, Wiley-Blackwell, 368 p., 2014.

Pfiffner, O. A.: Geology of the Alps. Chichester: Wiley-Blackwell, 376 pp, 2014.

Renard, P. Hytool: an open source matlab toolbox for the interpretation of hydraulic tests using analytical solutions, Journal of Open Source Software, 2(19), 441, doi:10.21105/joss.00441, 2017.

Rillard, J., Loisy, C., Le Roux, O., Cerepi, A., Garcia, B., Noirez, S., Rouchon, V., Delaplace, P., Willequet, O., and Bertrand, C.: The DEMO- CO_2 project: A vadose zone CO_2 and tracer leakage field experiment, International Journal of Greenhouse Gas Control, 39, 302-317, doi:10.1016/j.ijggc.2015.04.012, 2015.

Rinaldi, A. P., Guglielmi, Y., Zappone, A., Soom, F., Robertson, M., Cook, P., Kakurina, M., Wenning, Q., Rebscher, D., and Nussbaum, C.: Coupled processes in clay during tunnel excavation, EGU General Assembly Vienna, Austria, 4-8 May 2020, EGU2020-184, doi:10.5194/egusphere-egu2020-18041, 2020.

Rinaldi, A. P., Jeanne, P., Rutqvist, J., Cappa, F. and Guglielmi, Y.: Effects of fault-zone architecture on earthquake magnitude and gas leakage related to CO_2 injection in a multi-layered sedimentary system, Greenhouse Gases, 4(1), 99–120, 2014.

Rinaldi, A. P., Rutqvist, J., Finsterle, S., and Liu, H.H.: Inverse modeling of ground surface uplift and pressure with iTOUGH-PEST and TOUGH-FLAC: the case of CO_2 injection at In Salah Algeria, Computers & Geosciences, 108, 98-109, doi:10.1016/j.cageo.2016.10.009, 2017.

Rinaldi, A. P., and Rutqvist, J.: Modeling of deep fracture zone opening and transient ground surface uplift at KB-502 CO_2 injection well, In Salah, Algeria, International Journal of Greenhouse Gas Control, 12, 155–167, doi:10.1016/j.ijggc.2012.10.017, 2013.

Rinaldi, A. P., and Rutqvist, J.: Joint opening or hydroshearing? Analyzing a fracture zone stimulation at Fenton Hill, Geothermics, 77, 83-98. doi:10.1016/ 10.1016/j.geothermics.2018.08.006, 2019.

Roberts, J. J., and Stalker, L.: What have we learned about CO_2 leakage from field Injection tests? Energy Procedia, 114, 5711-5731, doi:10.1016/j.egypro.2017.03.1710, 2017.

Roques, C., Weber, U. W., Brixel, B., Krietsch, H., Dutler, N., Brennwald, M. S., Villiger, L., Doetsch, J., Jalali, M., Gischig, V., Amann, F., Valley, B., Klepikova, M., & Kipfer, R. In situ observation of helium and argon release during fluid-pressure-triggered rock deformation. Scientific Reports, 10(1), 6949, doi:10.1038/s41598-020-63458-x, 2020.

Rutqvist, J.: Status of TOUGH-FLAC simulator and recent applications related to coupled fluid flow and crustal deformations, Computers & Geosciences, 37, 739-750, 2011.

Rutqvist, J.: The Geomechanics of CO_2 storage in deep sedimentary formations, Geotechnical and Geological Engineering, 30, 525-551 doi:10.1007/s10706-011-9491-0, 2012.

Rutqvist, J., Rinaldi, A. P., Cappa, F., Jeanne, P., Mazzoldi, A., Urpi, L., Guglielmi, Y. and Vilarrasa, V.: Fault activation and induced seismicity in geological carbon storage – Lessons learned from recent modeling studies, Journal of Rock Mechanics and Geotechnical Engineering, 8, 789–804, doi:10.1016/j.jrmge.2016.09.001, 2016.

Schopper, F., Doetsch, J., Villiger, L., Krietsch, H., Gischig, V.S., Jalali, M., Amann, F., Dutler, N. and Maurer, H.: On the Variability of Pressure Propagation during Hydraulic Stimulation based on Seismic Velocity Observations, Journal of Geophysical Research: Solid Earth, 125, doi:10.1029/2019JB018801, 2020.

Schuster, K., Amann, F., Yong, S., Bossart, P., & Connolly, P.: High-resolution mini-seismic methods applied in the Mont Terri rock laboratory (Switzerland). Swiss Journal of Geosciences, 110(1), 213-231, 2017.

Skurtveit, E., Miri, R. and Hellevang, H.: Fluid-Rock Interactions in Clay-Rich Seals. In Geological Carbon Storage: Subsurface seals and caprock integrity (eds S. Vialle, J. Ajo-Franklin and J.W. Carey). doi:10.1002/9781119118657.ch8, 2018.

Shi, J.-Q., Smith, J., Durucan, S., Korre, A.: A Coupled Reservoir Simulation-geomechanical Modeling Study of the CO_2 Injection-induced Ground Surface Uplift Observed at Krechba, in Salah, Energy Procedia, 37, 3719–3726, 2013.

Tenthorey, E., Feitz, A., Credoz, A., Lavina, M. and Coene, E.: The CO2CRC Otway Controlled CO_2 Release Experiment in a Fault: Geomechanical Characterisation Pre-Injection, Proceedings of the Fifth International Conference on Fault and Top Seals, 1-5, doi:10.3997/2214-4609.201902321, 2019.

Vasco, D. W., Rucci, A., Ferretti, A., Novali, F., Bissell, R. C., Ringrose, P. S., Mathieson, A. S. and Wright, I. W.: Satellite-based measurements of surface deformation reveal fluid flow associated with the geological storage of carbon dioxide, Geophysical Research Letters, 37, L03303, doi:10.1029/2009GL041544, 2010.

Vasco, D. W., Bissell, R. C., Bohloli, B., Daley, T. M., Ferretti, A., Foxall, W., Goertz-Allmann, B. P., Korneev, V., Morris, J. P., Oye, V., Ramirez A., Rinaldi A. P., Rucci, A., Rutqvist J., White J., and Zhang, R.: Monitoring and Modeling Caprock Integrity at the In Salah Carbon Dioxide Storage Site, Algeria, in: Geological Carbon Storage: Subsurface Seals and Caprock Integrity, edited by Stéphanie, V., Ajo-Franklin, J. and Carey, J. W., 243–269, 2018.

Vialle, S. and Vanorio, T.: Laboratory measurements of elastic properties of carbonate rocks during injection of reactive CO_2 -saturated water, Geophysical Research Letters, 38, 2011.

Vilarrasa, V., and Carrera, J.: Geologic carbon storage is unlikely to trigger large earthquakes and reactivate faults through which CO_2 could leak, Proceedings of the National Academy of Sciences, 112(19), 5938-5943, doi:10.1073/pnas.1413284112, 2015.

Vilarrasa, V., Carrera, J., Olivella S., Rutqvist, J., and Laloui L.: Induced seismicity in geologic carbon storage, Solid Earth, 10, 871–892, 2019.

Vilarrasa, V. and Makhnenko, R. Y.: Caprock Integrity and Induced Seismicity from Laboratory and Numerical Experiments, Energy Procedia, 125, 494–503, 2017.

Vilarrasa, V., Rinaldi, A. P. and Rutqvist, J.: Long-term thermal effects on injectivity evolution during CO_2 storage, Int. International Journal of Greenhouse Gas Control, 64, 314–322, 2017.

Wenning, Q. C., Madonna, C., Kurotori, T., and Pini, R.: Spatial mapping of fracture aperture changes with shear displacement using X-ray computerized tomography, Journal of Geophysical Research: Solid Earth, 2019.

Wenning, Q. C., Madonna, C., and Zappone, A.: Anisotropic elastic properties and permeability of Opalinus shale from the 'Main Fault' and host formation within Mont Terri. 17th Swiss Geoscience Meeting, Fribourg, Switzerland, 2019.

Wenning, Q. C., Madonna, C., Kurotori, T., Pini, R., and Zappone, A.: Fracture aperture and flow evolution due to confined shear displacement using X-ray computerized tomography on crystalline and clay-rich rocks. 13th EURO – Conference on Rock Physics and Geomechanics, Potsdam, Germany, 2019.

Zappone, A., Rinaldi, A.P., Grab, M., Obermann, A., Claudio, M., Nussbaum, C. and Wiemer, S.: CO_2 Sequestration: Studying Caprock And Fault Sealing Integrity, The CS-D Experiment In Mont Terri , European Association of Geoscientists & Engineers, Conference Proceedings, Fifth CO_2 Geological Storage Workshop, Nov 2018, Volume 2018, p.1 – 5, https://doi.org/10.3997/2214-4609.201803002.

Zoback, M. D., and Gorelick, S.M.: Earthquake triggering and large-scale geologic storage of carbon dioxide, Proceedings of the National Academy of Sciences, 109(26), 10164-10168, doi:10.1073/pnas.1202473109, 2012.

Borehole-ID	Main Purpose	Diameter [mm]	Length [m]	Inclination [°]	Azimuth [°]
BCS-D1	Injection	101	23.4	0	0
BCS-D2	Fluid sampling, Pressure, pH and EC monitoring	101	18.6	0	0
BCS-D3	Active source seismic and ERT tomography	131	31.3	43	324
BCS-D4	Active source seismic and ERT tomography	131	36.4	42.5	323
BCS-D5	Micro-seismicity monitoring and active seismic	146	31.7	41	318
BCS-D6	Micro-seismicity monitoring	131	36.6	0	0
BCS-D7	Slip monitoring	116/101	30.5	0	0

Table 1: Parameters defining the CS-D boreholes: Inclination= deviation from the vertical (vertical = 0°); borehole depth is approximate 0.5m. The order of the boreholes in table represents the drilling sequence. The borehole BCS-D7 has an initial diameter of 116 mm from 0 to 13.60, and a diameter of 101 mm from 13.60 to 30.5 due to overcoring to retrieve a stuck drill bit.

	BCS-D1	BCS-D2	BCS-D4	BCS-D5	BCS-D6	BCS-D7
Top [m]	14.34	11.04	27.05	19.74	28.50	22.46
Dip dir [°]	133.40	125.70	158.60	334.10	121.80	126.70
Dip [°]	65.80	55.20	64.00	81.10	59.50	64.20
Bottom [m]	19.63	16.39	28.44	22.66	31.40	25.54
Dip dir [°]	138.60	138.20	149.80	155.30	123.60	150.30
Dip [°]	62.00	56.70	63.50	66.00	59.40	55.90

945 **Table 2: Main Fault geometry: Top = top of the Main Fault (middle point), Bottom =Bottom of the Main Fault (middle point); dip dir= direction from true North; due to poor image log quality in BCS-D3, no orientation could be identified.**

Interval	Test	Date (UTC+1)	Pressure range (MPa)	Comments	Est. T (m^2/s)
Q1	PST	11.03	1.2-2.0	Two series of ramp-up/ramp-down, then increased to 2 MPa and decay	N.E.
	SST	17.04	1.25-4.8	Steps 0.3 MPa every 10 minutes.	N.E.
	HP-SST	17.04	4.8-6.0	Steps 0.15 MPa every 5 minutes.	N.E.
	LST	15:48 17.04 - 14:30 18.04	4.8	Gradual step-down from HP-SST then single step for about 24 hours	N.E.
Q2	SST	04.02	1.0-3.8	Steps 0.2 MPa every 5 minutes. 20 minutes steps at 3.2 MPa and 3.8 MPa	N.E.
	LST1	18:57 27.02 – 00:35 10.03	1.2-3.6	Steps 0.3 MPa every 28-30 hours.	N.E.
	LST2	15:56 28.03 – 12:40 16.04	1.8-4.8	Steps 0.3 MPa every 28-30 hours. Last step lasted 172 hours.	N.E.
	HP-SST	16.04	4.8-6.0	Steps 0.15 MPa every 10 minutes.	N.E.
Q4	PST1	04.02	0.9-1.7	Two series of ramp-up ramp-down, then increased to 1.7 MPa and decay	1.8×10^{-13} (decay)
	LST	14:02 11.03 – 28.03 11.34	1.2-4.8	Steps 0.3 MPa every 28-30 hours.	2.8×10^{-13} (first step)
	HP-SST	28.03	4.8-6.0	Steps 0.15 MPa every 10 minutes. Last step for 1.5 hours.	4.0×10^{-13} (decay)
	PST2	16.04	1.8-4.2	Steps 0.3 MPa every 10 minutes.	6.8×10^{-13} (decay)
	PST3	11.06	1.2-4.8	Steps 0.3 MPa every 10 minutes. **Fault opening pressure (FOP) reached**.	9.2×10^{-12} (decay)

Table 3: Summary of all injection tests performed. Transmissivity has been estimated only for tests in injection interval Q4 of borehole BCS-D1 (N.E. stands for not estimated). We calculated transmissivity only for this interval, as only when injection occurred here there was a response in the monitoring borehole (BCS-D2). Note that the transmissivity was always estimated by modelling the injection pressure and never as cross-hole response

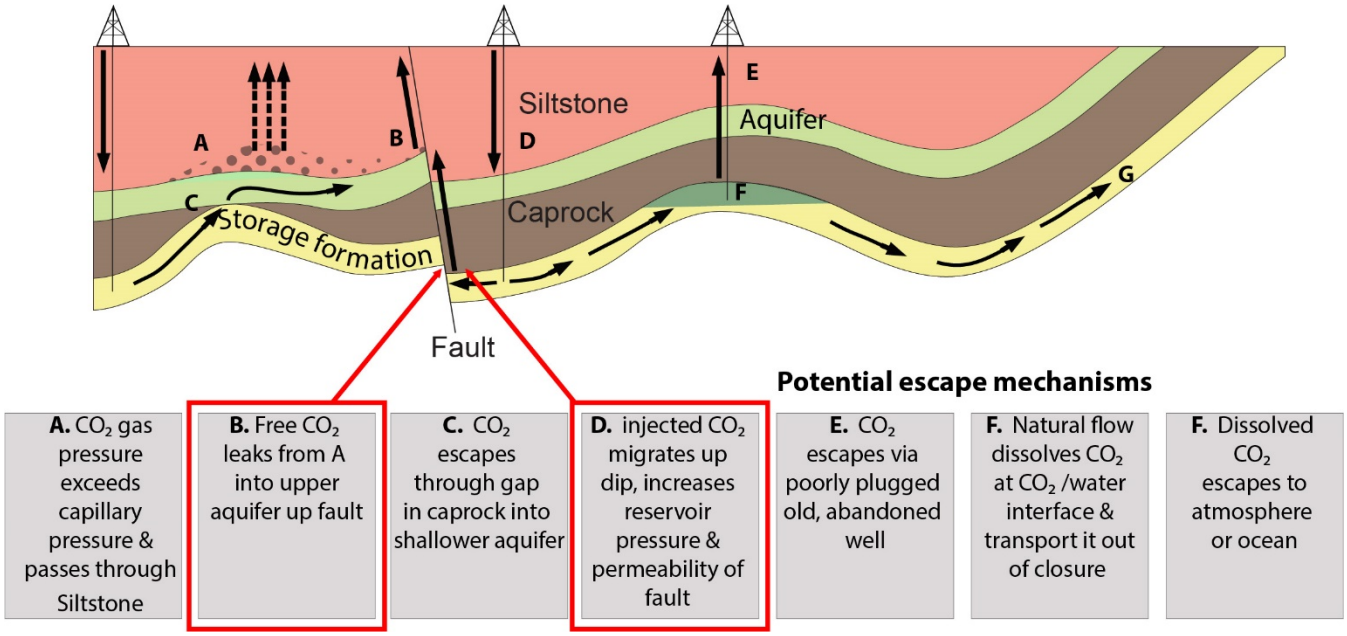

Figure 1: Potential leakage routes (modified after IPCCP Special report 2005). The scientific objective of the experiment is to better understand how the prolonged exposure to CO_2-rich water could affects the properties of a fault hosted in a caprock, altering its sealing properties (red arrows).

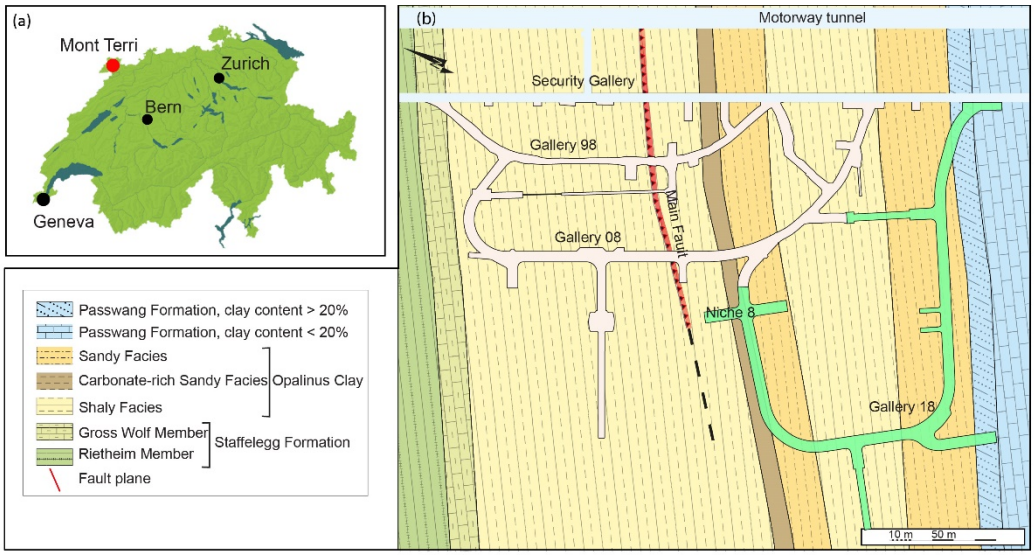
(a)
Mont Terri
Zurich
Bern
Geneva
(b)
Motorway tunnel
Security Gallery
Gallery 98
Main Fault
Gallery 08
Niche 8
Gallery 18
10 m
50 m
Passwang Formation, clay content > 20%
Passwang Formation, clay content < 20%
Sandy Facies
Carbonate-rich Sandy Facies
Shaly Facies
Opalinus Clay
Gross Wolf Member
Riethein Member
Staffelegg Formation
Fault plane

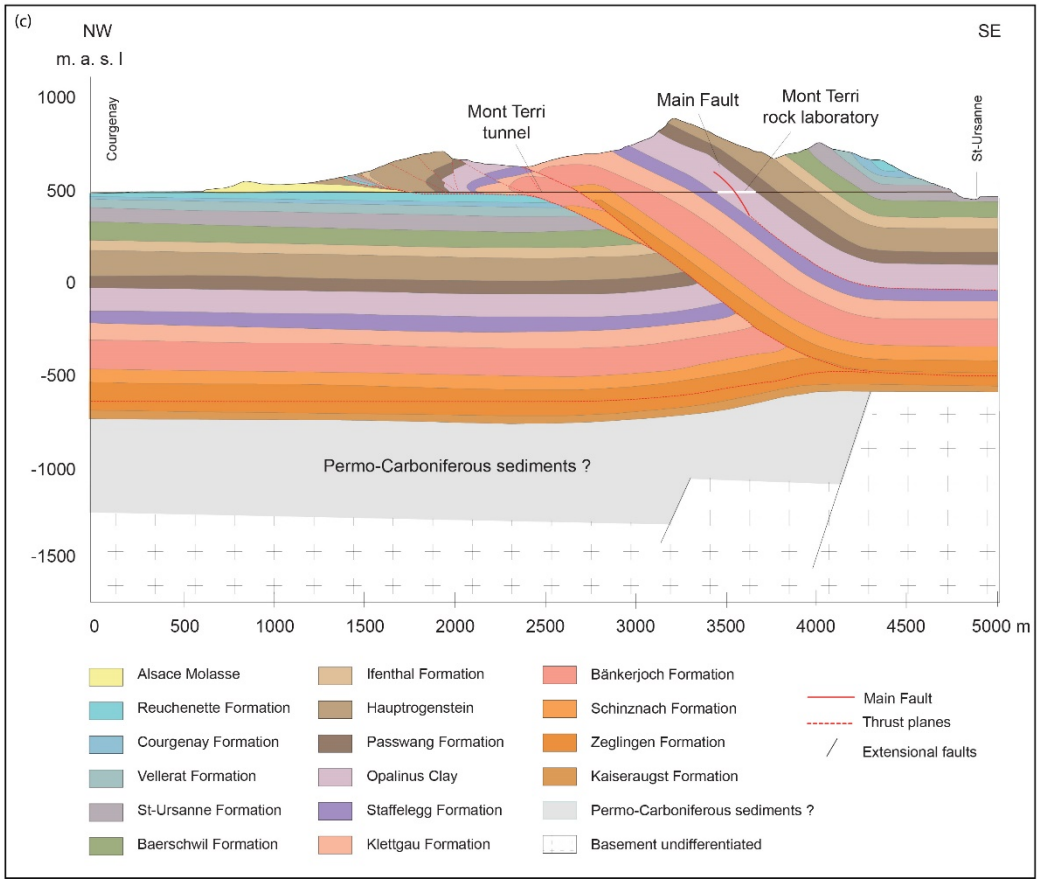
(c)
NW
SE
m. a. s. l
1000
500
0
-500
-1000
-1500
Courgenay
Mont Terri tunnel
Main Fault
Mont Terri rock laboratory
St-Ursanne
Permo-Carboniferous sediments ?
0
500
1000
1500
2000
2500
3000
3500
4000
4500
5000 m
Alsace Molasse
Reuchenette Formation
Courgenay Formation
Vellerat Formation
St-Ursanne Formation
Baerschwil Formation
Ifenthal Formation
Hauptrogenstein
Passwang Formation
Opalinus Clay
Staffelegg Formation
Klettgau Formation
Bänkerjoch Formation
Schinznach Formation
Zeglingen Formation
Kaiseraugst Formation
Permo-Carboniferous sediments ?
Basement undifferentiated
Main Fault
Thrust planes
Extensional faults

Figure 2: a) Location of the MTR. b) Schematic geological map of the laboratory area with the new tunnels in light green (after Trury and Bossart 1999). c) Geological interpretation of the main structures along a profile crosscutting the security gallery (Nussbaum et al., 2017).

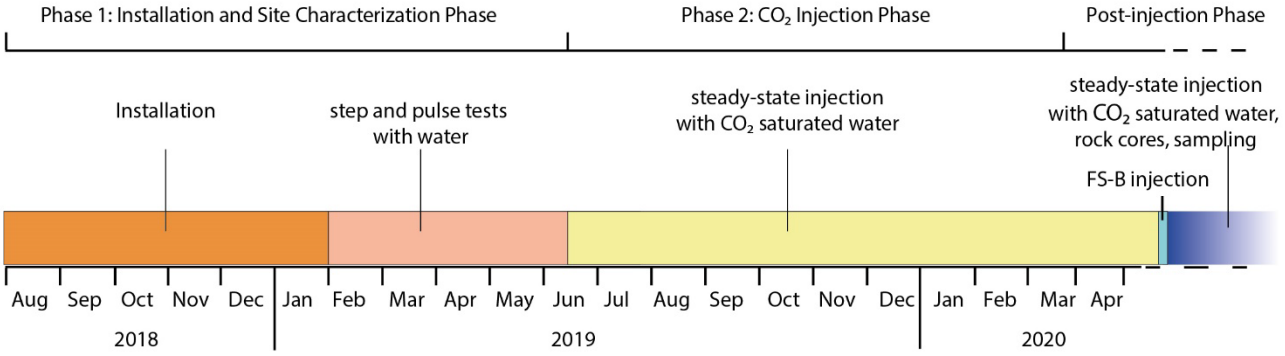

Figure 3: timeline of CS-D (the FS-B injection is at date postponed to a later stage).

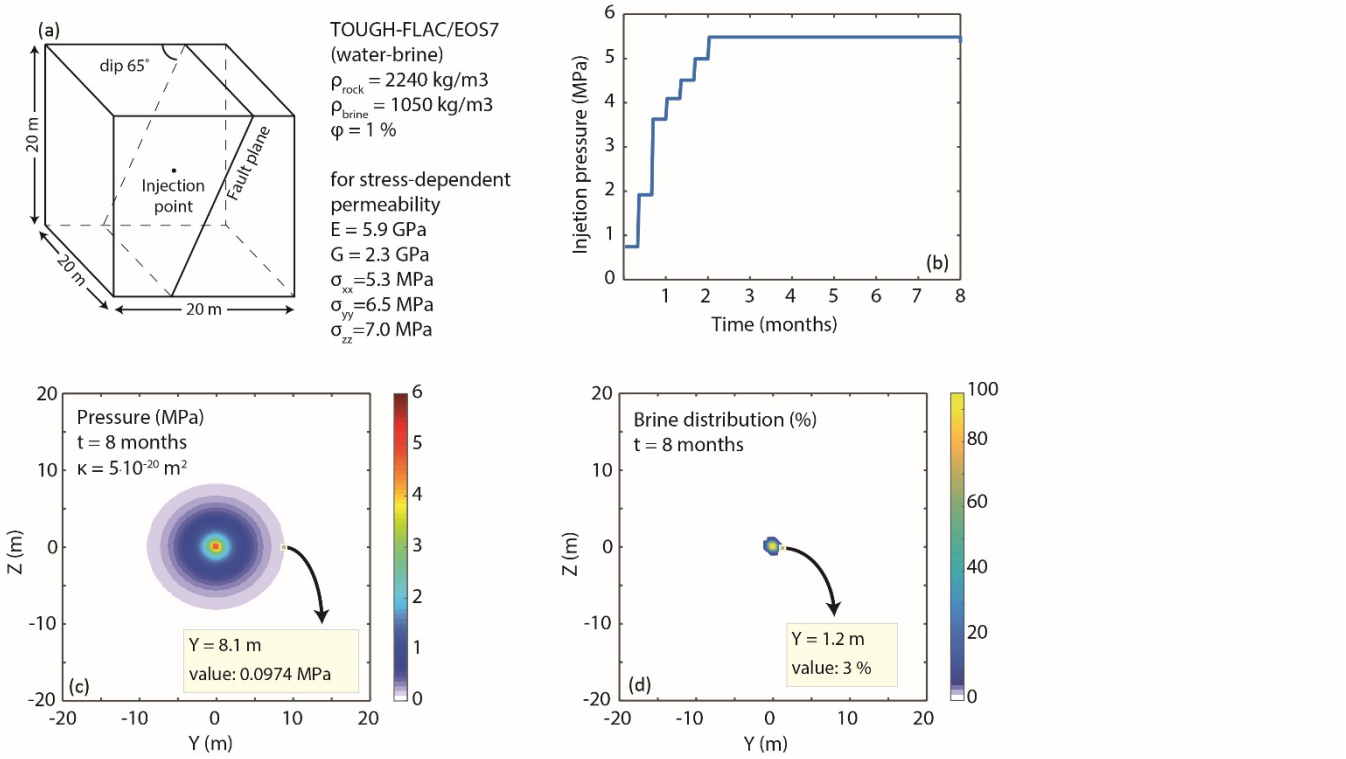

Figure 4: (a) Modelling domain and main properties. (b) The pressure at injection follows a step-wise behaviour with monthly increase. (c) Example of simulated distribution of pressure changes around the injection point after 8 months of constant head injection for permeability of $5{\cdot}10^{-20}$ m^2. (d) Simulated injected brine distribution after 8 months of constant head injection for permeability of $5{\cdot}10^{-20}$ m^2.

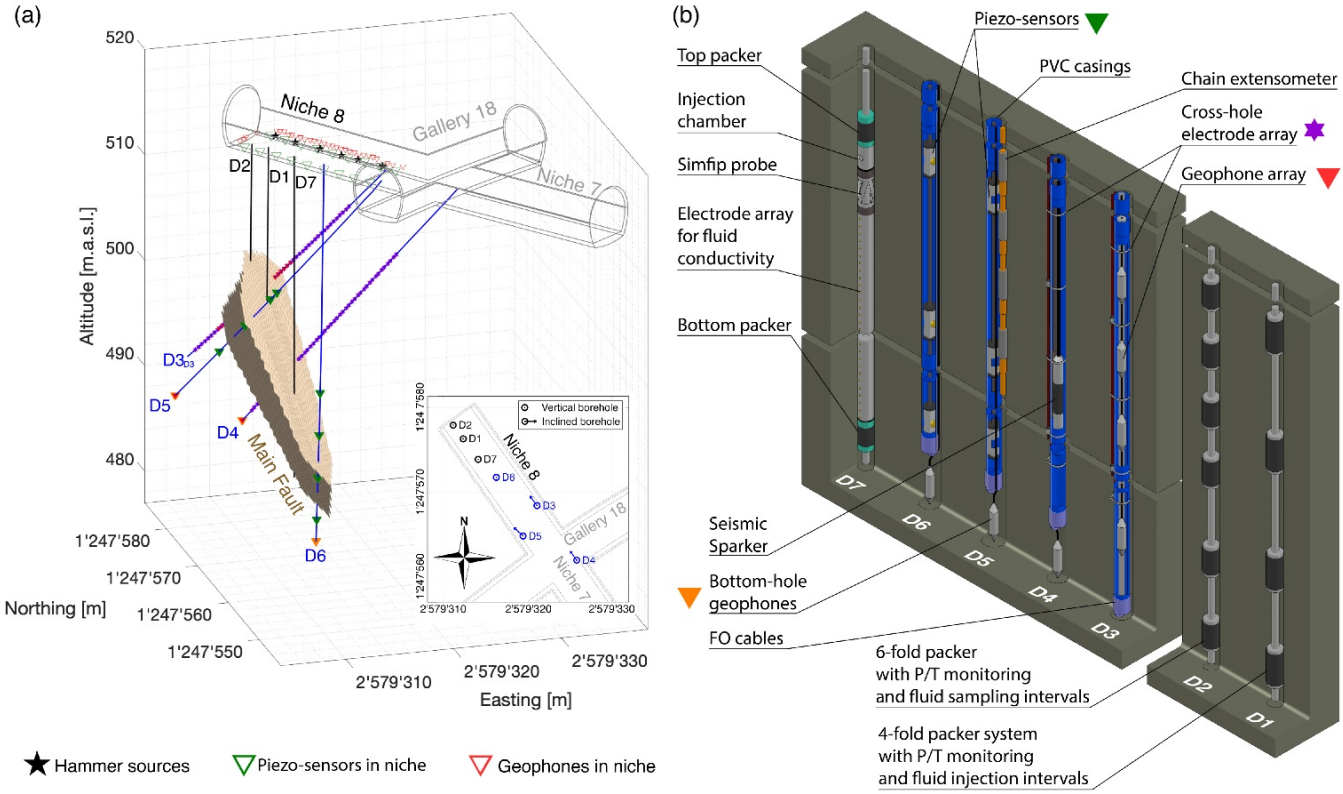

975 **Figure 5: a) Geometry of boreholes and of the Main Fault below niche 8; b) planar view of the borehole location in niche 8.**

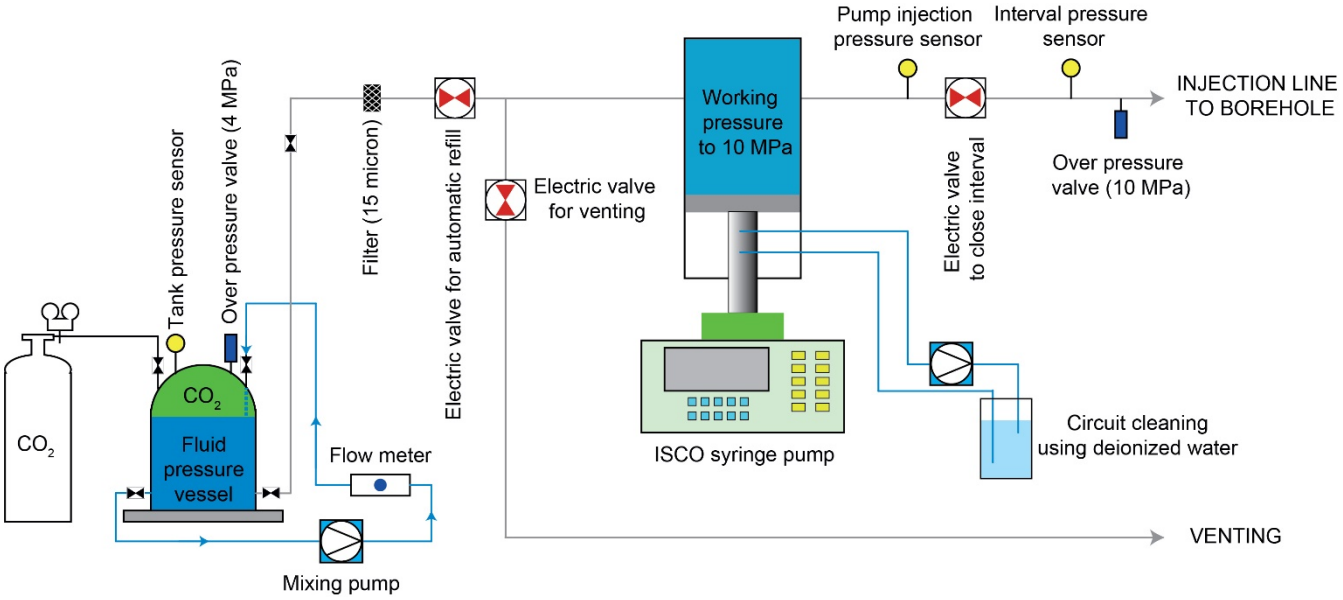

Figure 6: Injection system design for the CS-D experiment (modified after Solexperts AG, Switzerland)

980

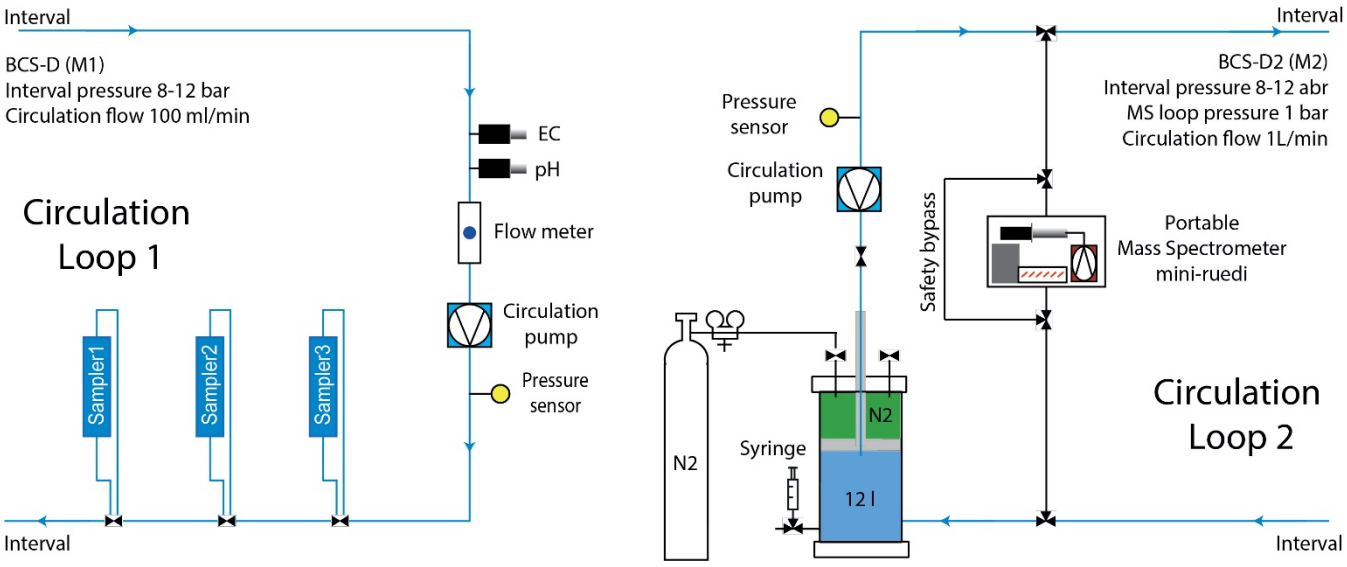

Figure 7: Circulation loops for the CS-D experiment (modified after Solexperts AG, Switzerland).

985

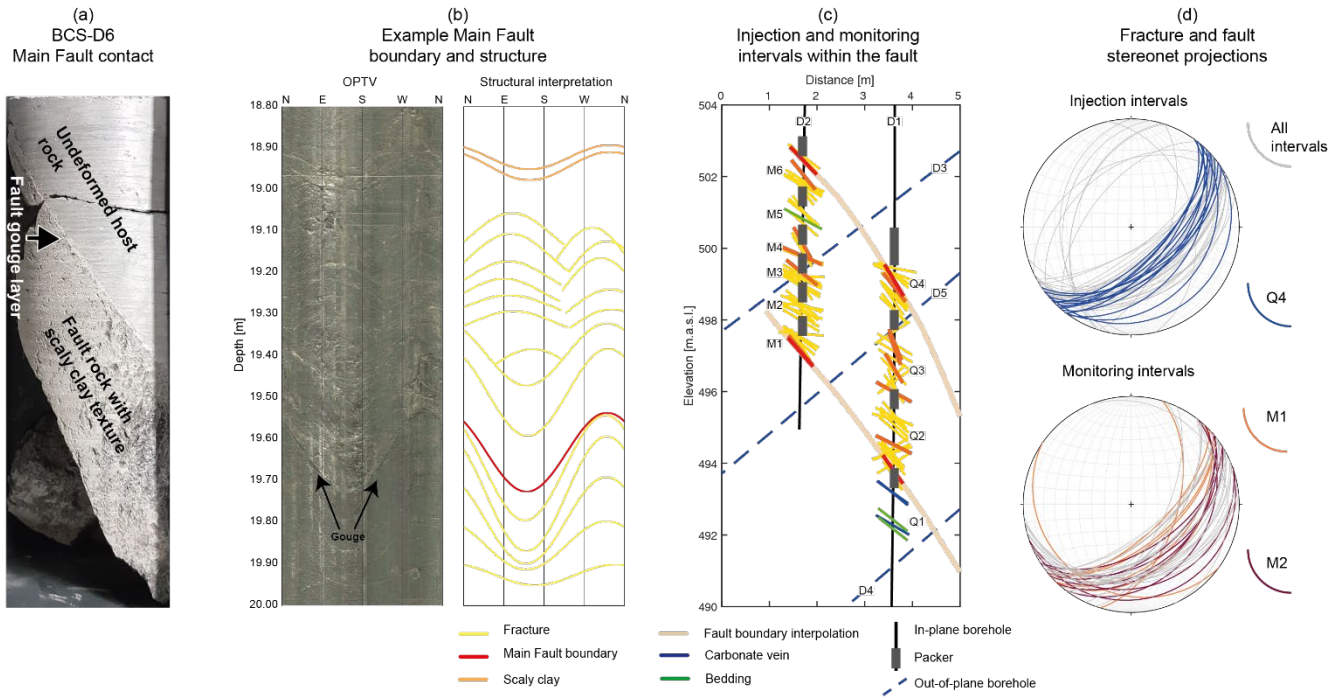

Figure 8: a) An example image log of the contact between the Main Fault and the host rock is shown. b) An example of the contact between the host rock and the Main Fault from core. c) Injection and monitoring intervals and mapped structures within the Main Fault boundaries. d) Fracture and fault stereonet projections within the injection borehole (top) and monitoring borehole (bottom). The stereonets highlight all the structures within the Main Fault (grey) and the structures from the injection interval Q4 (blue), monitoring interval M1 (orange), and monitoring interval M2 (red).

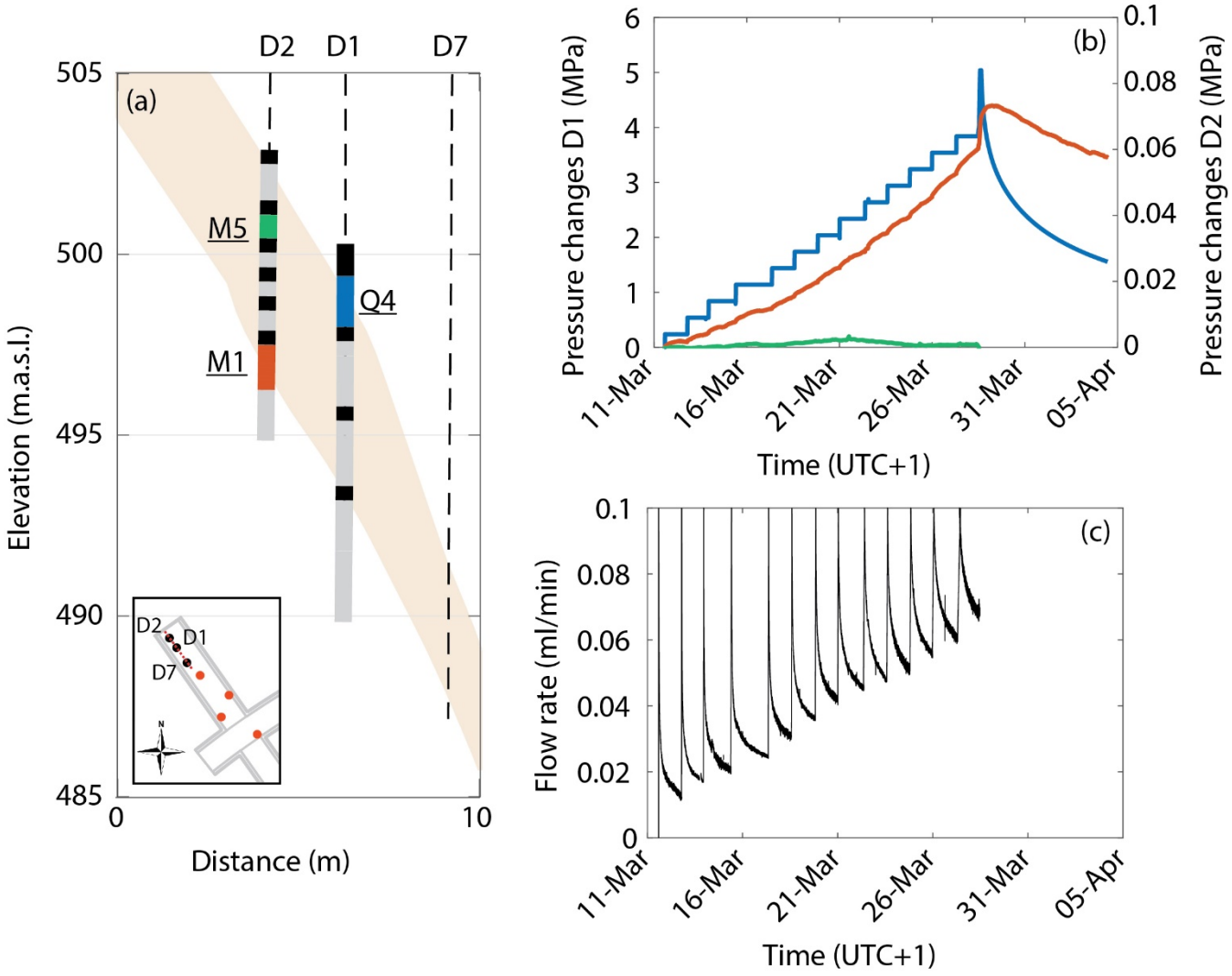

995 **Figure 9: a) Projection on plane of boreholes BCS-D1 and BCS-D2 and their intervals. The inlet shows the location of the boreholes and the orientation of the plane. b) Pressure changes in the injection interval Q4 (blue) and response at two intervals in the fluid monitoring borehole (M1 in red and M5 in green). The positions of the monitor intervals with respect the injection interval is shown in panel (a). c) Flow rate at the syringe pump.**

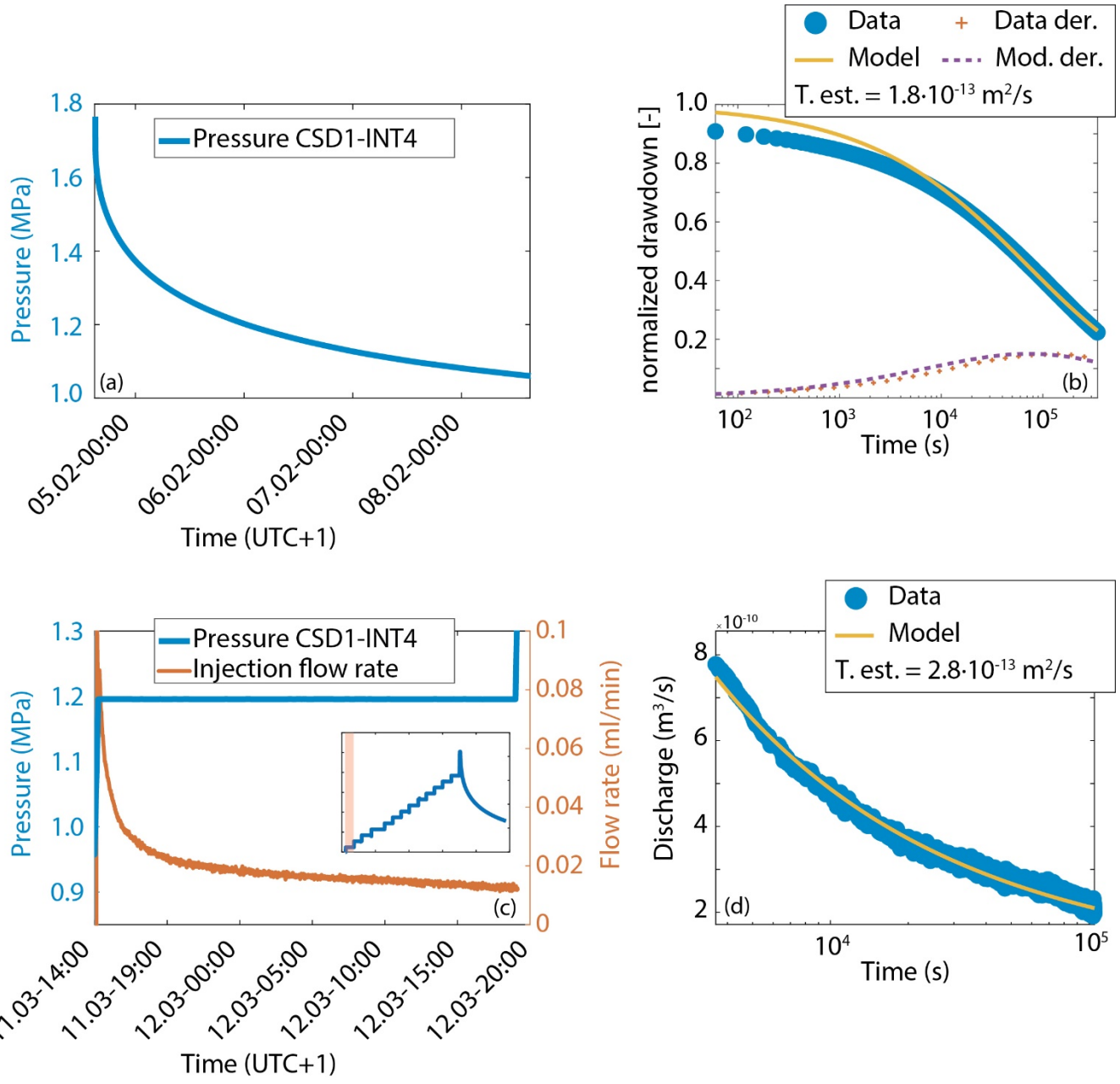

1000

Figure 10: a) Pressure decay after pulse in interval BCS-D1-Q4 (PST1). b) Analytical model and model derivative for pressure decay (Renard, 2017) and estimated transmissivity. c) First step of test LST in interval BCS-D1-Q4 (red is the flow rate, blue the pressure at injection). d) Analytical model of discharge (Renard, 2017) and estimate transmissivity.

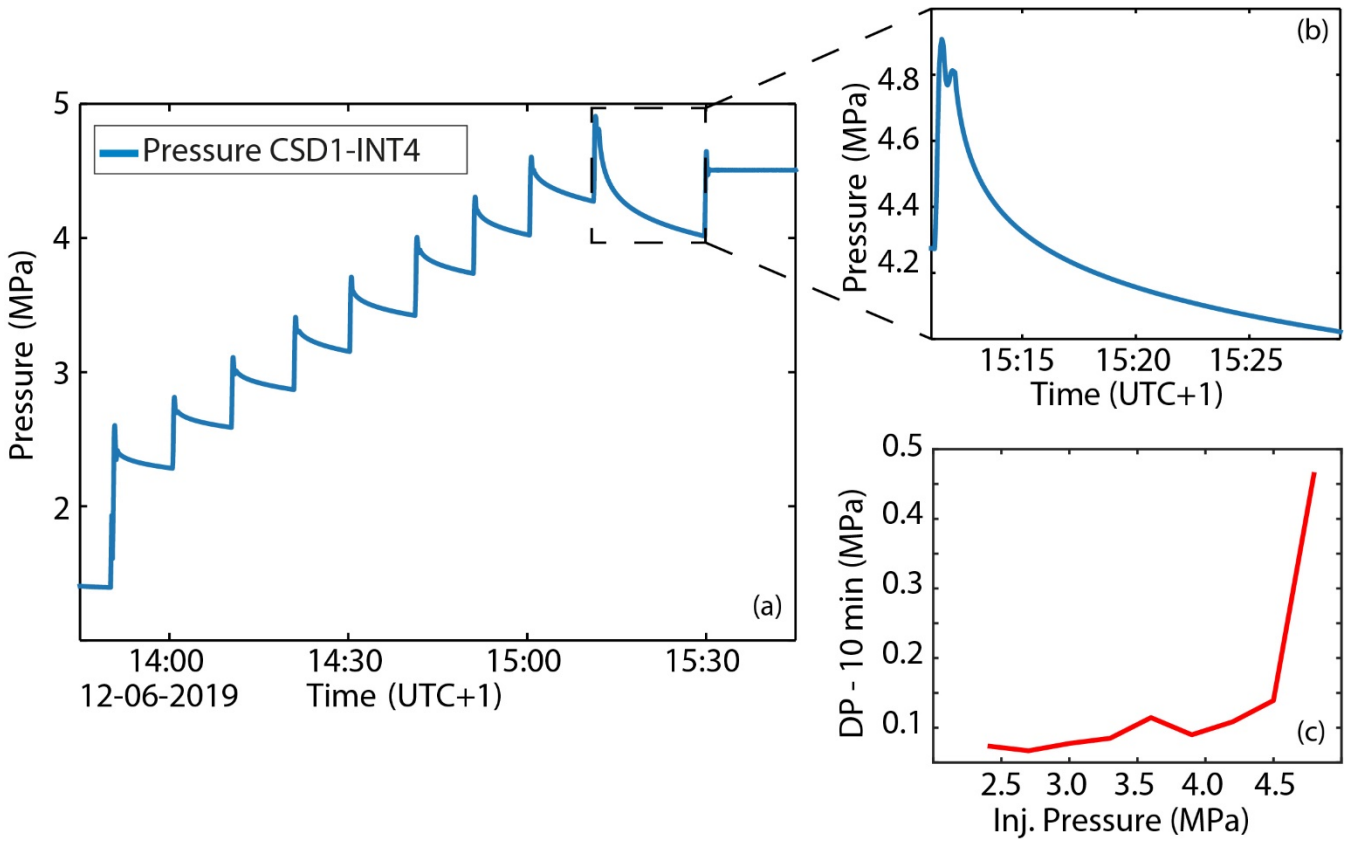

Figure 11: a) PST in interval BCS-D1-Q4 to determine fault opening pressure (FOP); b) enlarge view of the pressure drop after reaching opening conditions; note that the decay curve is much larger when the FOP is reached; c) pressure changes after the 10 minutes step vs injection pressure: the system is non-linear above 4.5 MPa injection pressure.

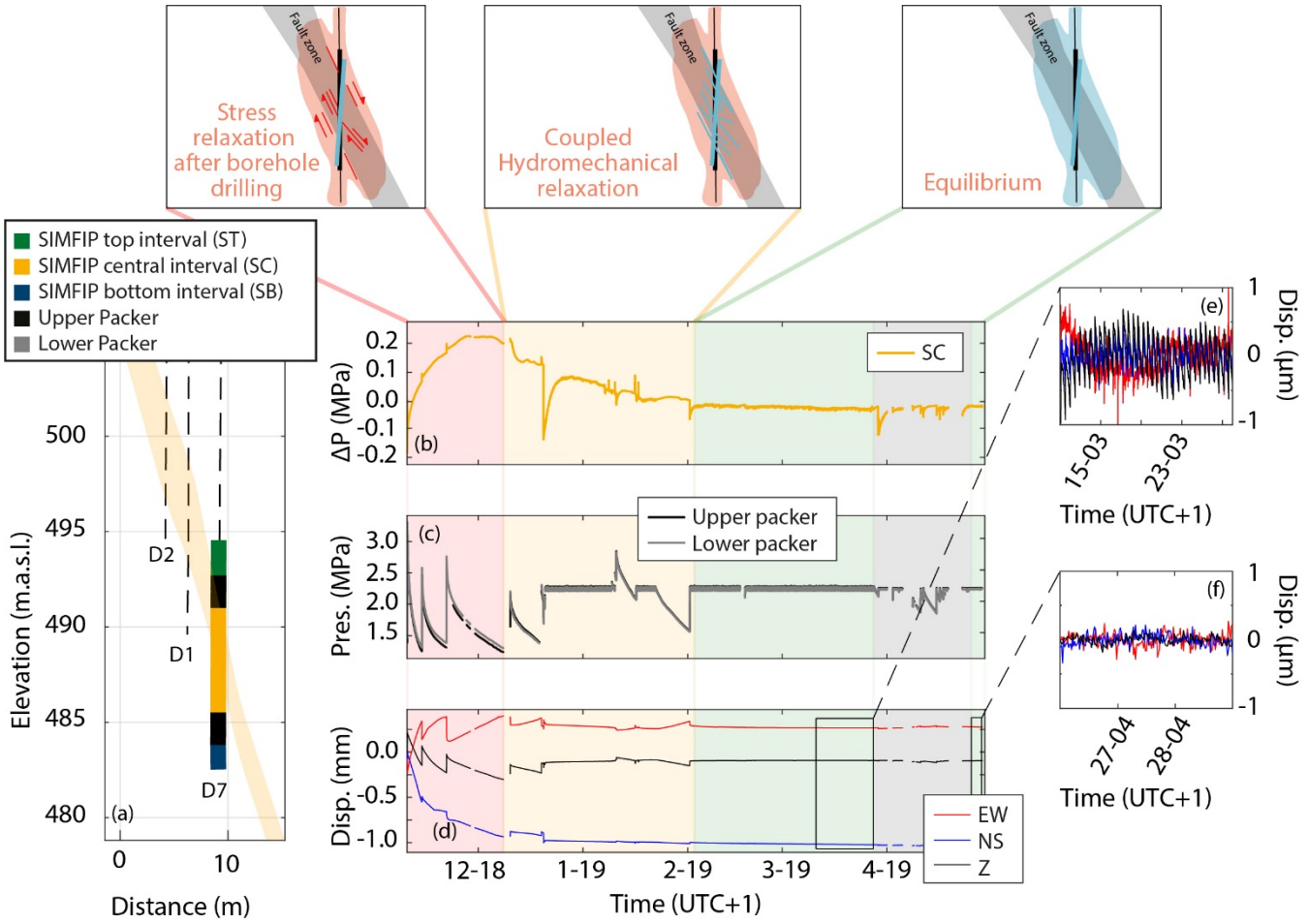

1015 **Figure 12: (a) Position of the SIMFIP probe across the fault zone in borehole BCS-D7. (b-d) Long-term fault zone displacement and pore pressure monitoring: (b) Interval pressure, (c) Packer pressure, (c) (EW, NS, Z) displacement of the upper packer of the SIMFIP probe (Fault hanging wall). (E, f) Enlargement of relative and detrended displacement monitoring in stable periods before and after packer pressure calibration.**

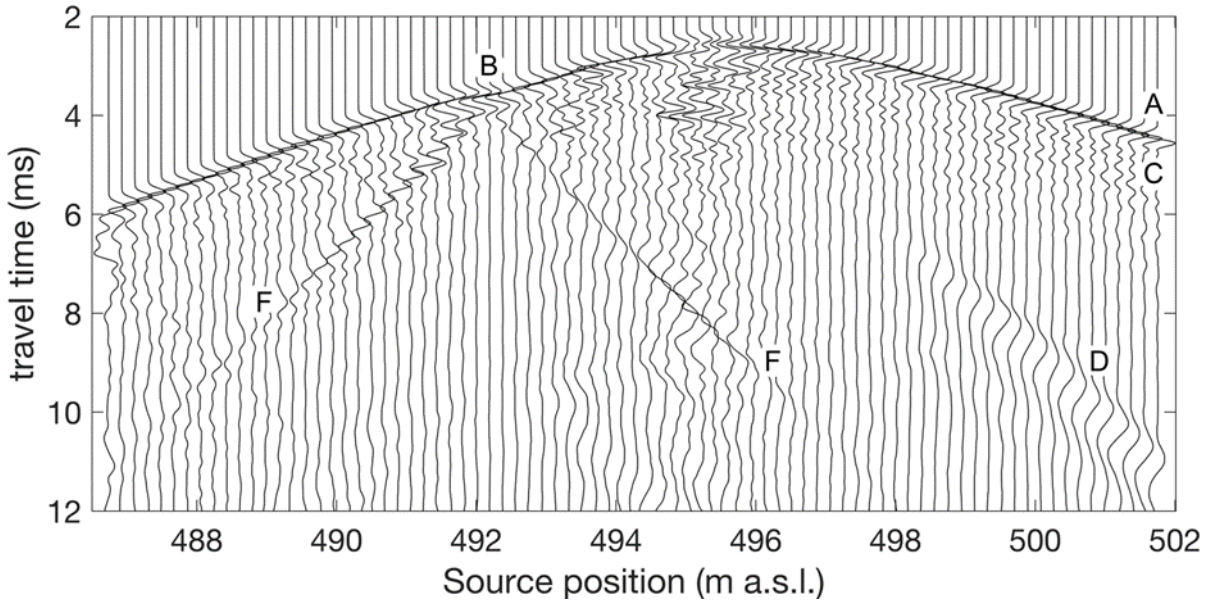

1020 **Figure 13: Common-receiver gather of processed seismic data, recorded with a cemented geophone in borehole BCS-D3, while a P-wave sparker source was employed at 25 cm intervals in borehole BCS-D4. . Labelled seismic events are the P-wave arrivals (A) with notable delay for sources fired within the Main Fault (B), slow and fast S-wave modes (C), tube wave propagating along the source borehole (D) and tube wave reflected at the Main Fault (F).**

1025

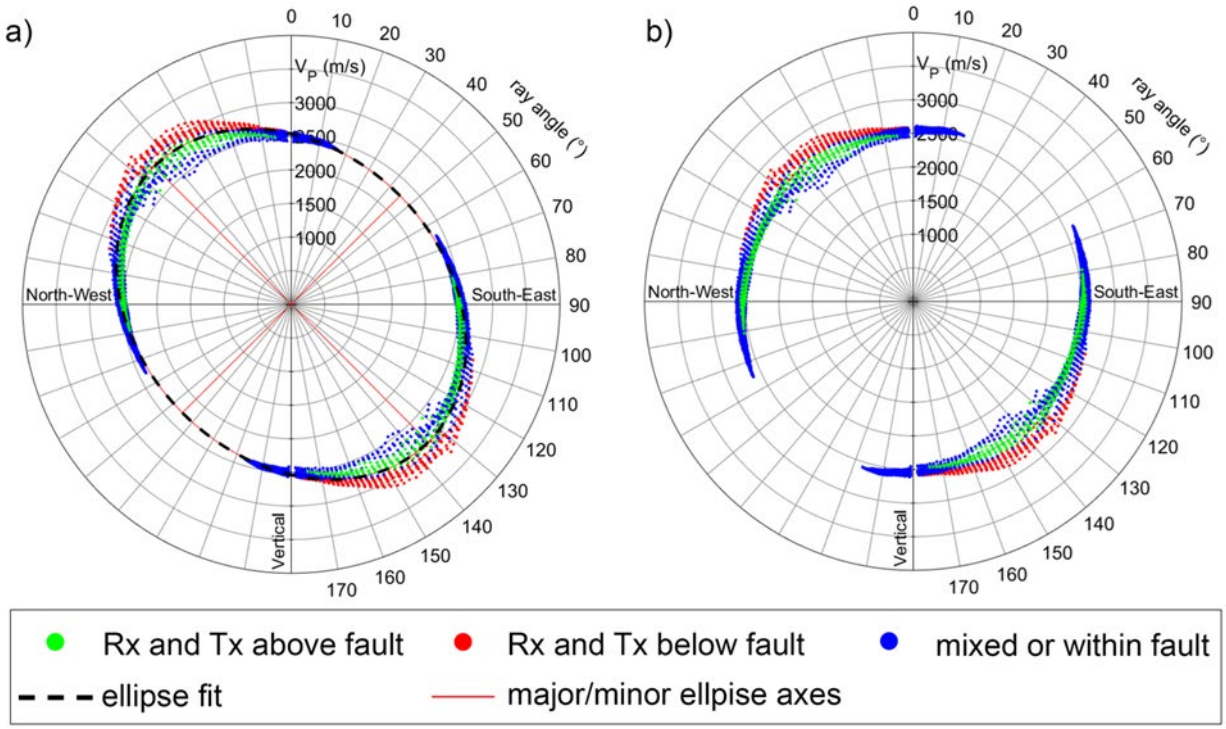

Figure 14: Average V_P for all receiver (Rx)-transmitter (Tx) pairs within the same plane as the one displayed in Figure 15. Since V_P shows a strong anisotropy (a), velocities were normalized (b) prior to performing the travel time inversion.

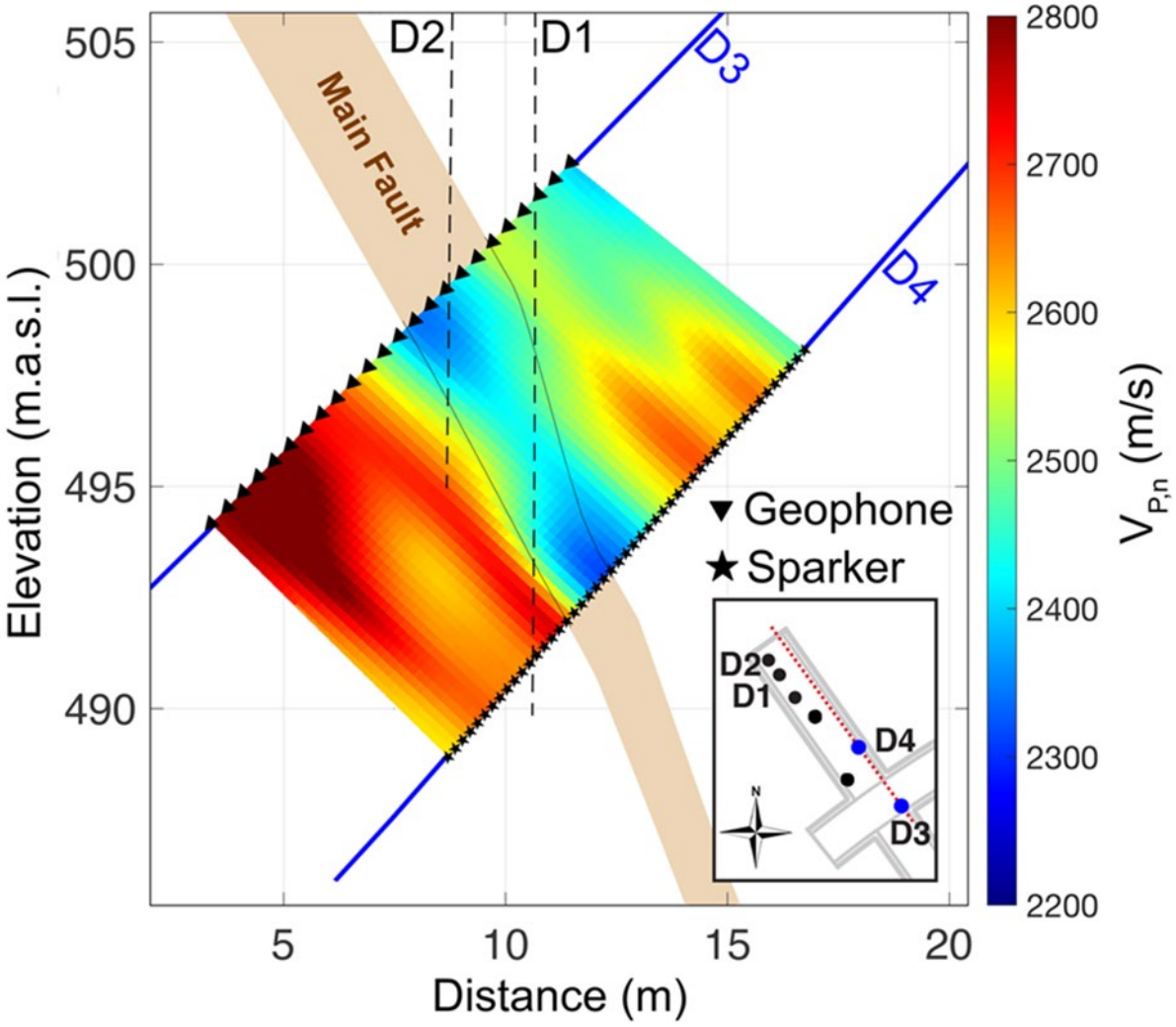

1030 **Figure 15: V_P-tomogram obtained by cross-hole travel time inversion between borehole BCS-D3 (geophones) and BCS-D4 (sparker sources). Locations of geophones and sources are indicated by triangle- and star-symbols, respectively**